# Redox Regulation of Brain Selective Kinases BRSK1/2: Implications for Dynamic Control of the Eukaryotic AMPK family through Cys-based mechanisms

George N. Bendzunas [1#,] Dominic P Byrne [2#,] Safal Shrestha [3], Leonard A Daly [2,4], Sally O. Oswald [2,4], Samiksha Katiyar [1], Aarya Venkat [1], Wayland Yeung [1,3], Claire E Eyers [2,4], Patrick A Eyers* [3], Natarajan Kannan* [1,2]

# Equal contributions

[1] Department of Biochemistry and Molecular Biology, University of Georgia, Athens, GA 30602, USA [2] Department of Biochemistry, Cell and Systems Biology, Institute of Systems, Molecular and Integrative Biology, University of Liverpool, Liverpool L69 7ZB, UK. [3] Institute of Bioinformatics, University of Georgia, Athens, GA 30602, USA. [4] Centre for Proteome Research, Institute of Systems, Molecular and Integrative Biology, University of Liverpool, Liverpool L69 7ZB, UK

*Correspondence to: Natarajan Kannan, Email: nkannan@uga.edu or Patrick Eyers, Email: patrick.eyers@liverpool.ac.uk

## Abstract

In eukaryotes, protein kinase signaling is regulated by a diverse array of post-translational modifications (PTMs). While regulation by activation segment phosphorylation in Ser/Thr kinases is well understood, relatively little is known about how oxidation of cysteine (Cys) amino acids modulate catalysis. In this study, we investigate redox regulation of the AMPK-related Brain-selective kinases (BRSK) 1 and 2, and detail how broad catalytic activity is directly regulated through reversible oxidation and reduction of evolutionarily conserved Cys residues within the catalytic domain. We show that redox-dependent control of BRSKs is a dynamic and multilayered process involving oxidative modifications of several Cys residues, including the formation of intra-molecular disulfide bonds involving a pair of Cys residues near the catalytic HRD motif and a highly conserved T-Loop Cys with a BRSK-specific Cys within an unusual CPE motif at the end of the activation segment. Consistently, mutation of the CPE-Cys increases catalytic activity *in vitro* and drives phosphorylation of the BRSK substrate Tau in cells. Molecular modeling and molecular dynamics simulations indicate that oxidation of the CPE-Cys destabilizes a conserved salt bridge network critical for allosteric activation. The occurrence of spatially proximal Cys amino acids in diverse Ser/Thr protein kinase families suggests that disulfide mediated control of catalytic activity may be a prevalent mechanism for regulation within the broader AMPK family.

## Introduction

Protein kinases are crucial components in cellular signaling networks, functioning as reversible molecular switches that orchestrate various biological processes. There are over 500 protein kinases encoded in the human genome that coordinate a wide range of cellular processes by catalyzing the transfer of a phosphate group from ATP to a hydroxyl group on the amino acid side chains of serine, threonine, or tyrosine residues in protein substrates (Manning et al. 2002). By catalyzing the reversible post-translational phosphorylation of Ser/Thr and Tyr residues of substrate proteins, protein kinases serve as signaling integrators that govern most aspects of eukaryotic life. Consequently, there exists a biological imperative to tightly control the catalytic activities of protein kinases, through cyclical phosphorylation of conserved amino acids, protein-protein interactions, and other regulatory post-translational modifications (PTMs). One essential mechanism governing kinase activity is the reversible phosphorylation of conserved amino acid residues within the activation loop (T-Loop) (Nolen, Taylor, and Ghosh 2004). In the inactive, unphosphorylated state, the T-Loop adopts a wide range of conformations, including conformations that obstruct substrate binding (Engh and Bossemeyer 2001). Phosphorylation of the activation loop induces an active spatial conformation that is typically more amenable to both binding and enzymatic phosphorylation of protein substrates, and this modification is prevalent across the kinase superfamily (Faezov and Roland L. Dunbrack 2023). Conversely, the removal of phosphate groups in this region by phosphatases (dephosphorylation) usually reverts kinases to an inactive state, generating a reversible switch to turn “on” and “off” kinase-dependent signaling pathways. More recently we hypothesized that ~10% of the Ser/Thr human kinome may also be subject to a conserved form of redox-dependent regulation, including key members of the CAMK, AGC, and AGC-like families of kinases through reversible oxidation of an evolutionarily conserved Cys residue, which lies adjacent to the critical regulatory phosphorylation site on the activation loop (T-loop +2 position) (Byrne et al. 2020).

Understanding the molecular mechanisms underlying kinase regulation by redox-active Cys residues is fundamental as it appears to be widespread in signaling proteins (Xiao et al. 2020; Corcoran and Cotter 2013; Cao et al. 2023) and provides new opportunities

to develop specific covalent compounds for the targeted modulation of protein kinases (Weisner et al. 2015). Moreover, redox-active Cys are major sensors of **R**eactive **O**xygen **S**pecies (ROS), such as superoxide and peroxide, which function as secondary messengers to regulate various cellular processes (Schieber and Chandel 2014 ;(Wani et al. 2011). In particular, the high cell permeability of $H_2O_2$ relative to other ROS species allows it to be sensed intracellularly by reactive Cys, which can differentially impact protein function and cellular localization (Lennicke et al. 2015; Rhee et al. 2005). Chemically accessible and reactive Cys residues can transition through several redox states, such as the transient sulfenic acid species (Cys-SOH) and higher order, 'irreversible', sulfinic and sulfonic forms (Cys-$SO_2H$ and Cys-$SO_3H$) (Forman et al. 2017; Gupta and Carroll 2014). Importantly, in the context of allosteric protein redox regulation, the sulfenic oxidized Cys species can form disulfide linkages with other reactive Cys residues, whilst a sulfenic derivative has also been observed to be stabilized through the formation of a cyclic sulfenamide for tyrosine phosphatase PTP1B (van Montfort et al. 2003; Salmeen et al. 2003). The chemical reactivity, and thus biological susceptibility, of an individual Cys residue to oxidative modification is contingent on the intrinsic p$K_a$ value (where $K_a$ is the acid dissociation constant), which in turn is influenced by networks of interacting amino acids (including phosphorylated amino acids), solvent accessibility, protein-protein interactions, and protein structural dynamics (Poole 2015; Xiao et al. 2020; Soylu and Marino 2016). Unlike phosphorylation, which allosterically communicates with distal sites through positively charged residues that coordinate the phosphate group, it is largely unclear how the redox state of a T-loop localized Cys residue may alter the catalytic activity of a kinase (Garrido Ruiz et al. 2022), although a change in the activation segment conformation is a likely outcome, as demonstrated by careful analysis of Ser/Thr kinases, notably members of the AGC-family kinase AKT (Su et al. 2019).

The human AMPK-related kinase (ARK) family, consisting of 14 members (termed BRSK1-2, NUAK1-2, SIK1-3, MARK1-4, MELK, and AMPKα1 and AMPKα2) are fundamental regulators of cellular metabolism, growth, differentiation, and polarity (Shao et al. 2014; Byrne et al. 2020; Shirwany and Zou 2014; Zmijewski et al. 2010), and BRSK1/2 function upstream of redox-based signaling to the pleiotropic transcription

factor Nrf2 (Tamir, Drewry, et al. 2020; Tamir, Bowman, et al. 2020). Like other ARK members, BRSK1/2 possess similar structural organization, consisting of an N-terminal serine/threonine catalytic (kinase) domain, which is followed by a ubiquitin-associated (UBA) domain, a C-terminal spacer, and in some members, a kinase-associated (KA1) domain (Bright, Thornton, and Carling 2009) (Fig 1a). In addition to sharing structural homology, all ARKs (except for MELK) are known to be activated by phosphorylation on their T-Loop by the common upstream regulator LKB1, which is constitutively active in cells (Lizcano et al. 2004). All of the ARKs contain an activation loop 'T-loop + 2 Cys' residue, which can be prognostic for redox regulation (Byrne et al. 2020), and the catalytic activities of several members have been demonstrated experimentally to be modulated by ROS, including the nominative member, AMPKα, which is both directly and indirectly regulated by redox-state (Auciello et al. 2014; Hinchy et al. 2018; Choi et al. 2001; Shirwany and Zou 2014; Shao et al. 2014). However, the precise mechanisms whereby various ARKs are regulated under redox conditions remain obscure and are likely to be context specific.

The Brain Specific Kinases (BRSKs, also termed Synapses of Amphids Defective [SAD] kinases), consist of two paralogs in vertebrates, termed BRSK1 and BRSK2, and are among the least well-studied of the ARK family (Nie et al. 2012). However, like all other members of the ARK family, BRSKs are downstream signaling targets of the Ser/Thr kinase LKB1 and also have the potential to be regulated by CAMKII, PAK1, and PKA, suggesting signal-dependent phosphorylation as a central regulatory mechanism (Alessi, Sakamoto, and Bayascas 2006; Lizcano et al. 2004; Nie et al. 2012; Bright, Carling, and Thornton 2008). BRSKs are highly expressed in the brain and central nervous system of model organisms, where they exhibit both distinct and redundant molecular functions (Kishi et al. 2005; Nakanishi et al. 2019); furthermore, they are implicated in several human pathologies, in particular neurodevelopmental disorders such as autism spectrum disorder (Saiyin et al. 2017; Li et al. 2020; Deng et al. 2022).

In the current study, we identify a new dominant mechanism for regulation of BRSKs through oxidative modification of conserved Cys residues within the kinase domain. We demonstrate that the catalytic activities of both BRSK1 and BRSK2 are fine-tuned

through oxidative modification of the T-Loop +2 Cys residue, which communicates with a BRSK-specific Cys residue in the APE motif (CPE in BRSKs) within the activation segment. We provide evidence that the T-Loop Cys forms disulfide bonds with the 'CPE' motif Cys and that mutating the CPE-Cys to an alanine increases BRSK activity relative to the wild-type (WT) enzyme. Using a combination of biochemical analysis, structural modeling, and molecular dynamics simulations, we identify regulatory roles for these BRSK-conserved Cys residues and characterize novel intramolecular disulfide-links, providing new insights into BRSK1/2 regulation and the broader AMPK family regulation. Together, these findings highlight complex regulatory processes for BRSK1/2 that are dependent on both phosphorylation and Cys-redox modulation, with broad implications for the other members of the ARK family.

# Methods

## Recombinant proteins and general reagents

All purchased biochemicals were of the highest purity available, and all recombinant proteins were analyzed by intact mass-spectrometry to confirm the species present. Active, recombinant full-length BRSK1 (2-778) and BRSK2 (2-674) proteins purified from insect Sf21 cells were purchased from MRC PPUU reagents (University of Dundee). Active recombinant LKB1/STRADα/MO25α was purchased from Merck. Gateway pENTR plasmids encoding full length human BRSK1 & BRSK2 were generated as part of the NIH common fund initiative to Illuminate the Druggable Genome (IDG) and was a gift from Dr. Ben Major (Washington University, St. Louis). Antibodies for BRSK1, BRSK2, DYKDDDDK (D6WB5) Tag, Phospho-AMPKα (Thr172), HA-Tag (C29F4), 6XHiS tag and GAPDH were from Cell Signaling Technology. Antibodies for Phospho-Tau and GFP were from Invitrogen. The glutathione antibody was obtained from Abcam.

## Cloning, Gateway Recombination and Site Directed Mutagenesis

LR Clonase ligation of the Gateway pENTR plasmids into pDest vectors encoding both Flag and HA tags was performed as follows. The Entry clones encoding full length BRSKs were subjected to LR recombination reactions with the respective pDest vectors encoding both Flag and HA tags using the Gateway LR Clonase II enzyme mix, according to the manufacturer's instructions. BRSKs were also cloned into a pcDNA3 vector using standard a standard T4-ligase (NEB) protocol and expressed in frame with a 3C-protease cleavable N-terminal tandem STREP-tag. The catalytic domains of BRSK1$^{29\text{-}358}$ or BRSK2$^{14\text{-}341}$ were sub-cloned into pET28a (Novagen) to generate N-terminal hexa-His tagged plasmid constructs for expression of BRSK1/2 catalytic domains in *E. coli*. Site-directed mutagenesis was performed using standard PCR-based mutagenic procedures with the Q5 Site-Directed Mutagenesis Kit (New England Biolabs) following the manufacturer's instructions. All plasmids were validated by complete sequencing of the protein coding region.

## Recombinant BRSK expression and purification

Recombinant human BRSK1$^{29-358}$ or BRSK2$^{14-341}$ proteins, or indicated amino acid substitutions, were produced in BL21 (DE3) pLysS *E. coli* cells (Novagen). BRSK1/2 expression was induced with 0.5 mM isopropyl-β-D-thiogalactopyranoside (IPTG) for 18 h at 18°C and N-terminal His6-tag fusion proteins purified by step-wise affinity chromatography and size exclusion chromatography using a HiLoad 16/600 Superdex 200 column (GE Healthcare) equilibrated in 50 mM tris-HCl (pH 7.4), 100 mM NaCl, and 10% (v/v) glycerol. Where appropriate for redox assays, recombinant proteins were purified under reducing conditions in the presence of 1 mM DTT, as previously described (Byrne et al. 2020). BRSK proteins expressed from bacteria are unphosphorylated and catalytically inactive, and were activated by incubation with 10 ng of purified LKB1/STRADα/MO25α holoenzyme complex in the presence of 1 mM ATP and 10 mM $MgCl_2$ for 18 h at 4°C. Phosphorylation of BRSK proteins was verified by mass spectrometry and/or Western blotting analysis using a pThr$^{172}$ AMPKα antibody, which demonstrates cross-reactivity for BRSK1/2 T-Loop phosphorylation (Tamir et al. 2020).

## Detection of glutathionylated proteins by immunoblotting

Recombinant BRSK1 and 2 (0.5 µg) were incubated with 50 mM Tris-HCl (pH 7.4) and 100 mM NaCl, with 10 mM GSSG or GSH for 30 min at 20°C, and glutathione-protein complexes were detected by immunoblotting after nonreducing SDS-PAGE.

## BRSK1/2 Kinase assays

BRSK activity assays were performed using microfluidic real-time mobility shift-based assays, as described previously (Byrne et al. 2020; Byrne et al. 2016; Mohanty et al. 2016), in the presence of 2 µM of the fluorescent-tagged BRSK1/2 peptide substrate (AMARA; 5-FAM- AMARAASAAALARRR -COOH) and 1 mM ATP. Optimal pressure and voltage settings were established to improve separation of phosphorylated and nonphosphorylated peptides. All assays were performed in 50 mM Hepes (pH 7.4), 0.015% (v/v) Brij-35, and 5 mM $MgCl_2$, and the real-time or end point degree of peptide phosphorylation was calculated by differentiating the ratio of the phosphopeptide:peptide. BRSK1/2 activity in the presence of different redox reagents was quantified by monitoring the generation of phosphopeptide during the assay,

relative to controls. Data were normalized with respect to control assays, with phosphate incorporation into the peptide generally limited to <20% to prevent depletion of ATP and to ensure assay linearity. Recovery of BRSK activity from oxidative inhibition was assessed by incubating BRSKs with 1 mM hydrogen peroxide, followed by infusion of 2 mM DTT and substrate phosphorylation monitoring in real time. To account for potential variability in LKB1-dependent phosphorylation of BRSK proteins, rates of kinase activity (calculated as pmol phosphate incorporation per min) for each protein was normalized by densitometry to the activation site of phosphorylation signal (established with pThr$^{172}$ AMPKα antibodies and ImageJ software).

**Differential Scanning Fluorimetry**

Thermal shift assays were performed with a StepOnePlus real-time polymerase chain reaction (PCR) machine (Life Technologies) using SYPRO Orange dye (Invitrogen) and thermal ramping (0.3°C in step intervals between 25° and 94°C). All proteins were diluted to a final concentration of 5 μM in 50 mM tris-HCl (pH 7.4) and 100 mM NaCl in the presence or absence of 10 mM DTT and were assayed as described previously (Foulkes et al. 2018). Normalized data were processed using the Boltzmann equation to generate sigmoidal denaturation curves, and average $T_m/\Delta T_m$ values were calculated as previously described (Murphy et al. 2014) using GraphPad Prism software.

**Human cell culture and treatment**

HEK-293T cells were cultured in Dulbecco's modified Eagle medium (Lonza) supplemented with 10% fetal bovine serum (HyClone), penicillin (50 U/ml), and streptomycin (0.25 μg/ml) (Lonza) and maintained at 37°C in 5% $CO_2$ humidified atmosphere.

To examine the effects of oxidative stress on BRSK activity, cells were transiently co-transfected for 24 h with plasmids for expression of full-length, N-terminal tagged (Flag, HA or tandem Strep tag) BRSK1/2 (or Cys-Ala mutants) and GFP-TAU (Addgene), using 3:1 polyethylenimine (average $M_w$, ~25,000 Da; Sigma-Aldrich) to total DNA ratio (4 μg BRSK and 2 μg TAU DNA) in a single well of a 24-well culture plate. To investigate inactivation of BRSK by peroxide, cells were incubated for 20 min with 10 mM $H_2O_2$, or

buffer control. To establish reversibility of oxidative inhibition, cells were incubated for 20 min with 10 mM $H_2O_2$, or buffer control followed by a 15 min incubation with 20 mM reduced glutathione (GSH). In all assays, cells were subsequently washed 3x in PBS, harvested in bromophenol blue–free SDS sample buffer supplemented with 1% Triton X-100, protease inhibitor cocktail tablet, and a phosphatase inhibitor tablet (Roche), or in lysis buffer (50 mM Tris-HCl (pH 7.4), 150 mM NaCl, 1 mM EDTA with 10 % (v/v) glycerol and 1 % (v/v) Triton X-100, with 1X protease inhibitor cocktail and 1X HALT phosphatase inhibitor). Lysates were sonicated briefly and clarified by centrifugation at 20 817×*g* for 20 min at 4°C, and supernatants were sampled and diluted 30-fold for calculation of the protein concentration using the Coomassie Plus Staining Reagent (Bradford) Assay Kit (Thermo Fisher Scientific). Cell lysates were normalized for total protein concentration and processed for immunoblotting or immuno-precipitation (IP).

**Liquid chromatography mass spectrometry (LC-MS) analysis BRSKs**

48 h post-transfection, HEK-293T cells overexpressing BRSK1 and 2 (containing an N-terminal 3C cleavable tandem STREP-tag) were treated with 1 mM of the cell permeable chemical oxidant pervanadate for 30 min. Cells were resuspended in ice cold lysis buffer (50 mM Tris-HCl (pH 6.5), 150 mM NaCl, 10 % (v/v) glycerol, 1 % (v/v) NP-40, 100 mM iodoacetamide) and disrupted by passing the cell suspension through a 25-gauge needle 10 times. Lysates were clarified by centrifugation at 20 817×g for 20 min at 4°C, and recombinant proteins were affinity precipitated using Step-TACTIN beads and physically eluted using 3C protease for subsequent MS analysis. Affinity precipitated BRSK1/2 and bacterially derived recombinant proteins (10 µg) were diluted (~4-fold and ~18-fold respectively) in 100 mM ammonium bicarbonate (pH 8.0) containing 10 mM iodoacetamide and incubated in the dark for 30 min at room temperature. Samples were subjected to an SP3-based trypsin digestion protocol (adapted from, (Daly et al. 2023)), using 100 mM ammonium bicarbonate (pH 8.0) and 0.5 µg of Trypsin gold (Promega). Digested fractions were split 50/50, and one half was treated with dithiothreitol and iodoacetamide as previously described by (Ferries et al. 2017). Samples were then subjected to in-house packed strong-cation exchange stage tip clean up, as described by (Daly et al. 2021). Dried peptides were solubilized in 20 µl

of 3% (v/v) acetonitrile and 0.1% (v/v) TFA in water, sonicated for 10 min, and centrifuged at 13,000x *g* for 15 min at 4 °C prior to reversed-phase HPLC separation using an Ultimate3000 nano system (Dionex) over a 60-min gradient, as described by (Ferries et al., 2017). For affinity precipitated BRSK preparations from human cells, all data acquisition was performed using a Thermo QExactive mass spectrometer (Thermo Scientific), with higher-energy C-trap dissociation (HCD) fragmentation set at 30% normalized collision energy for 2+ to 4+ charge states. MS1 spectra were acquired in the Orbitrap (70K resolution at 200 *m/z*) over a range of 300 to 2000 *m/z*, AGC target = 1e6, maximum injection time = 250 ms, with an intensity threshold for fragmentation of 1e3. MS2 spectra were acquired in the Orbitrap (17,500 resolution at 200 *m/z*), maximum injection time = 50 ms, AGC target = 1e5 with a 20 s dynamic exclusion window applied with a 10 ppm tolerance. For bacterially derived recombinant proteins, all data acquisition was performed using a Thermo Fusion Tribrid mass spectrometer (Thermo Scientific), with higher-energy C-trap dissociation (HCD) fragmentation set at 32% normalized collision energy for 2+ to 5+ charge states. MS1 spectra were acquired in the Orbitrap (120K resolution at 200 *m/z*) over a range of 400 to 2000 *m/z*, AGC target = 100%, maximum injection time = auto, with an intensity threshold for fragmentation of 2.5e4. MS2 spectra were acquired in the Orbitrap (30k resolution at 200 *m/z*), maximum injection time = dynamic, AGC target = auto with a 20 s dynamic exclusion window applied with a 10 ppm tolerance. For disulfide analysis (regardless of sample type), raw data files were converted into mgf format using MSConvert, with peak picking filter set to “2- ” and searched with the MASCOT search engine (Perkins et al. 1999); searching the UniProt Human Reviewed database (updated weekly, accessed January 2023) (UniProt 2023) with variable modifications = carbamidomethylation (C), oxidation (M), phosphorylation (ST), instrument type = electrospray ionization–Fourier-transform ion cyclotron resonance (ESI-FTICR) with internal fragments from 200-2000 *m/z*, MS1 mass tolerance = 10 ppm, MS2 mass tolerance = 0.01 Da. The crosslinking option was selected for the accessions Q8TDC3 or Q8IWQ3 with strategy set to Brute-force, for InterLink, IntraLink and LoopLink for the linker “Xlink: Disulfide (C)”. For the best MASCOT scoring peptide spectrum match (PSM) for a disulfide-containing peptide, the mgf file was extracted from the raw file and imported into a custom R script for re-

drawing and manual annotation. Immunoprecipitated samples were additionally analyzed using PEAKS Studio (version XPro) using the same database, mass tolerances and modifications as previously described. PEAKS specific search settings: instrument = Orbi-Orbi, Fragmentation = HCD, acquisition = DDA, De Novo details = standard and a maximum of 5 variable PTMs possible. PEAKS PTM mode was enabled and filtering parameters of De Novo score >15, -log10P(value) >30.0, Ascore >30.0.

## Phylogenetic Analysis

We identified and aligned diverse BRSK-related sequences from the UniProt reference proteomes database (downloaded on June 7, 2022) (UniProt 2023) using MAPGAPS (Neuwald 2009). From these hits, we manually curated a diverse set of sequences, then inferred a maximum-likelihood phylogenetic tree with IQ-TREE version 2.0.7 (Minh et al. 2020). Branch support values were generated using ultrafast bootstrap (Hoang et al. 2018) with 1000 resamples. The optimal substitution model was LG+R6 based on the Bayesian Information Criterion as determined by ModelFinder (Kalyaanamoorthy et al. 2017). The consensus tree was used as our final topology. Subsequent analyses were performed using the ETE3 Toolkit (Huerta-Cepas, Serra, and Bork 2016).

## Molecular Dynamics Simulations

The starting model for molecular dynamics (MD) simulations was selected to provide an accurate representation of the protein kinase in its active-like conformation. To achieve this, we utilized an AlphaFold model of the BRSK2 kinase domain, corresponding to residues 14-267, in an active-like conformation. The average pLDDT score for the portion of the AlphaFold model employed in MD simulations was calculated to be 89.18%, indicating high confidence and accuracy (Jumper et al. 2021). Starting structures were prepared using the CHARMM-GUI interface which allowed for incorporation and parameterization of T-Loop phosphorylation, cysteine to alanine mutation, and oxidative cysteine modification (Brooks et al. 2009; Lee et al. 2016; Jo et al. 2014). Cysteine 176 (T+2) and 183 (CPE motif) were each mutated to alanine, sulfenic acid, or sulfonic acid forms. The protein was solvated in a cubic box of TIP3P

water molecules, and counterions were added to maintain neutrality. The final systems contained ~ 54,000 atoms.

Prior to production runs, the system was subjected to minimization and equilibration protocols, using previously described parameters (Yeung et al. 2021; Venkat et al. 2023). Initially, a steepest descent energy minimization was performed to relax the system, followed by equilibration at constant volume and temperature (NVT) and constant pressure and temperature (NPT). Each equilibration stage was carried out for 125 ps with 1 fs time steps. Following equilibration, long-range electrostatics were calculated via particle mesh Ewald (PME) algorithms using the GROMACS MD engine (Van Der Spoel et al. 2005). Three 100 ns production molecular dynamics (MD) replicates were conducted at a 2 fs time-step using the CHARMM36 forcefield for each starting model (Brooks et al. 2009). The resultant MDs were visualized with PyMOL (Schrodinger 2015) and analyzed in the python environment (Michaud-Agrawal et al. 2011).

**SDS-PAGE and Western blotting**

Processed cell lysates and purified recombinant proteins were loaded onto 10% (v/v) SDS-PAGE gels, separated by electrophoresis and transferred onto nitrocellulose membranes using a semi-dry transfer system at 300 mA for 45 minutes. Nitrocellulose membranes were blocked with 4% (w/v) Bovine Serum Albumin (BSA, Rockland) in Tris-buffered saline with 0.1% (v/v) Tween-20 (TBST) for 1 h at room temperature and incubated overnight at 4°C with the indicated primary antibodies. Protein was detected using specific secondary IRdye conjugated antibodies (Donkey anti Rabbit IRdye800cw or Goat anti Mouse IRdye680) and imaged using LI-COR Odyssey imaging system, or HRP-conjugated secondary antibodies and enhanced chemiluminescence reagent (Pierce ECL Plus, Thermo Fisher Scientific). All antibodies were prepared in a solution of BSA dissolved in TBST and diluted according to manufacturer's instructions. Reducing and non-reducing SDS-page for BRSK proteins was performed as previously described (Byrne et al, 2020). Phospho-Tau signal intensities were quantified using the intensity of pTau:total Tau (GFP) normalized to GAPDH signal as calculated by Image Studio software (LI-COR Biosciences). Statistical analysis was conducted in GraphPad

Prism, to determine significant differences between experimental groups. Data is presented as mean ± standard error of the mean (SEM).

**Size Exclusion Chromatography with multi-angle Light scattering (SEC-MALS)**

The oligomeric state of recombinant BRSKs was characterized by in-line Size Exclusion Chromatography-Multi-Angle Laser Light Scattering (SEC-MALS). Purified BRSK proteins (1 mg $mL^{-1}$) were applied directly to a HiLoad 16/60 Superdex 200 attached to an ÄKTA pure fast protein liquid chromatography (FPLC) system equilibrated in 10 mM Tris-HCl pH 7.4, 150 mM NaCl at a flow rate of 0.7 mL $min^{-1}$. Eluted protein was detected by a MALLS detector and a differential refractive index (DRI) detector (DAWN HELEOS-II and Optilab TrEX; Wyatt Technology, Santa Barbara, CA, USA). Data was analyzed using ASTRA v6.1 software (WYATT). The system was calibrated using BSA prior to data collection.

## Results

### Full-length BRSKs exhibit Redox-Sensitivity

The catalytic output of purified full length human BRSK1 & 2 (Fig 1a) was monitored in real-time using a microfluidic kinase assays system and a generic ARK family substrate peptide AMARA (5-FAM- AMARAASAAALARRR -COOH), which is phosphorylated by BRSK1/2, but not the upstream kinase LKB1. In the absence of reducing agents (buffer alone), detectable peptide phosphorylation was extremely low for both kinases and ablated in the presence of $H_2O_2$ (Fig 1b). In contrast, inclusion of DTT enhanced BRSK1 & 2 activity by several orders of magnitude. Moreover, $H_2O_2$-dependent inhibition of catalysis could be reversed, and even increased relative to basal activity, with the subsequent addition of a bolus of the reducing agent DTT. BRSK proteins were rapidly activated by DTT in a concentration-dependent manner, suggesting an obligate requirement of an appropriate reducing environment in order to enable catalytic activity (Fig 1c). Similarly, basal BRSK activity was inhibited by a gradient of $H_2O_2$ (Fig 1d). We next attempted to validate these *in vitro* observations in a human cell line. As there are currently no suitable endogenous substrates known to be specifically or exclusively phosphorylated by BRSK1 or 2, or that are not regulated by redox themselves (Tamir et al. 2020), we employed a GFP-Tau overexpression system in HEK-293T cells to monitor intracellular BRSK activity. BRSKs have previously been shown to increase the phosphorylation of Tau at Ser 262 (Yoshida and Goedert 2012). Consistently, co-expression of full length, N-terminal FLAG-tagged BRSK1 and 2 with GFP-Tau resulted in robust Tau phosphorylation (pTau), whilst pTau signal was abrogated in a kinase dead control (BRSK1/2 KD) where the catalytic aspartate residue within the 'HRD' motif ($D146^{BRSK1}$ or $D141^{BRSK2}$) was mutated to an alanine (Fig 1e). Active BRSKs have previously been shown to increase the phosphorylation of Tau on sites that include Ser 262 (Yoshida and Goedert 2012), and BRSK1/2 phosphorylation of Tau is potentially dysregulated in Alzheimer's disease (Morshed et al. 2021). Western blotting also revealed a dose-dependent and statistically significant decrease in BRSK-mediated pTau signal following incubation of HEK-293T cells with peroxide for 10 minutes, with little alteration in total transfected Tau protein (Fig 1f). At the highest concentrations of

peroxide treatment, we detected a reduction in total BRSK protein levels, suggesting a potential loss of stability for both kinases. Importantly, $H_2O_2$-dependent loss of pTau could be reversed following exposure of the cells to the physiological antioxidant glutathione (GSH) (Fig 1g). These findings suggest that reversible oxidative modulation is relevant to BRSK1/2 kinase-dependent signaling in human cells, which can be recapitulated *in vitro*.

## Mass spectrometric evidence that BRSK cysteine pairs can form intramolecular disulfide bonds

To identify residues that may contribute to redox regulation of BRSKs, we analyzed tryptic peptides derived from precipitated full-length cellular BRSK1 and BRSK2 by liquid chromatography–tandem mass spectrometry (LC-MS/MS). HEK-293T cells transiently over-expressing Strep-tagged BRSK proteins were lysed in the presence of the alkylating agent iodoacetamide to covalently block free thiol groups. LC-MS/MS revealed the presence of intramolecular bonds between $C147^{BRSK1}$ - $C153^{BRSK1}$ and $C191^{BRSK1}$ - $C198^{BRSK1}$ and $C132^{BRSK2}$ - $C138^{BRSK2}$ and $C176^{BRSK2}$ - $C183^{BRSK2}$ (Fig 2a). Of note, all identified disulfide forming Cys residues were located in the kinase domains of the two proteins, in close proximity to known catalytic or regulatory motifs. $C147^{BRSK1}$ - $C153^{BRSK1}$ and $C132^{BRSK2}$ - $C138^{BRSK2}$ structurally link the HRD motif in the catalytic loop to the preceding E-helix, and $C191^{BRSK1}$ - $C198^{BRSK1}$ and $C176^{BRSK2}$ - $C183^{BRSK2}$ couple the T-loop Cys to the Cys residue of the CPE motif in BRSK1/2 (equivalent to the APE motif in most kinase activation segments) (Fig 2b). To study these reactive Cys residues in the context of catalysis, we purified the unphosphorylated catalytic domain of human $BRSK1^{29-358}$ or $BRSK2^{14-341}$ to homogeneity from *E. coli*. As expected, both truncated variants of BRSK were completely inactivate in our AMARA-based kinase assay but could be 'switched on' following incubation with the physiological upstream regulator LKB1 (Fig 2c). Of note, despite sharing ~95% sequence identity within their kinase domain, LKB1-activated BRSK2 had higher catalytic activity compared to BRSK1 (Fig 2c). Moreover, and in support of our previous findings for full-length BRSK proteins (Fig1), incubation of LKB1-activated WT BRSK1 or 2 with DTT greatly increased activity.

These data are consistent with regulatory Cys-based modification of the kinase domain under oxidative conditions, which can be reversed with a reducing agent *in vitro*.

**Emergence and structural location of cysteines residues in BRSK proteins**

Reversible redox regulation of signaling proteins typically requires sulfenyl derivatization of an exposed Cys residue(s) (Heppner, Janssen-Heininger, and van der Vliet 2017). Cys is the second least abundant amino acid in the vertebrate proteome, and conserved surface exposed Cys side chains can function as redox "hotspots" (Fomenko, Marino, and Gladyshev 2008; Su et al. 2019; Xiao et al. 2020). Previously, we established that all 14 members of the ARK family kinases, including BRSK1 and 2, contain a T-loop + 2 Cys residue. This residue is equivalent to the redox sensitive C199 found in PKA (Humphries, Juliano, and Taylor 2002) and is prognostic of redox regulation for multiple human Ser/Thr kinases (Byrne et al., 2020). Of the ARK family kinases that we previously analyzed, AMPKα1, SIK1-3 and MELK were all acutely inhibited by $H_2O_2$ in a reversible manner *in vitro*, which we attributed to sulfenylation of the activation segment Cys, based on biochemical and evolutionary analysis (Byrne et al., 2020). The T-loop + 2 Cys corresponds to $C191^{BRSK1}$ and $C176^{BRSK2}$ in BRSK1 and 2 respectively. This residue is located within the canonical activation segment, in close proximity to the regulatory site of LKB1 phosphorylation. Interestingly, mapping of Cys residues across the human ARK family reveals several conserved Cys located throughout their kinase domains (Fig 3a and b). However, these studies also reveal a distinguishing Cys residue that is unique to the catalytic domain of human BRSKs, which is located at the canonical alanine position of the "APE" motif, converting it to "CPE" ($C198^{BRSK1}$/ $C183^{BRSK2}$ (Fig 3b). Of note, the unusual CPE Cys forms an intramolecular disulfide with the T-loop +2 Cys (Fig 2a). Intramolecular dimers incorporating T-loop Cys have also been identified in MELK and AKT2 (Cao et al. 2013; Huang et al. 2003). MELK is exceptional in that it possess both a T-loop +1 as well as a T-loop +2 Cys, where the T-loop +1 Cys forms an intramolecular disulfide with a Cys proximal to the DFG motif and the T-loop +2 can form an intermolecular disulfide potentiating dimerization (Cao et al. 2013). In the case of AKT2, the T-loop +2 Cys forms an intramolecular disulfide with a Cys equivalent to that seen in MELK (Huang et al. 2003). In addition to the T+2 Cys,

most human ARK family members (with the exception of MELK) contain an additional conserved Cys positioned 7 residues upstream of the HRD motif (HRD -7 Cys) located in the E-helix (Fig 3a and b). BRSKs share the HRD -7 Cys ($C147^{BRSK1}$/ $C132^{BRSK2}$), but further diverge from other ARK family members with the insertion of an additional potential disulfide bond-forming Cys residues preceding the HRD motif in the catalytic loop (CHRD-Cys, $C153^{BRSK1}$/ $C138^{BRSK2}$ in Fig 3a and b).

**Phylogenetic analysis of BRSK protein sequences**

A careful analysis reveals the emergence of an early BRSK1 variant, which we term 'proto-BRSK1' that distinguishes it from the closely related AMPKs (Supp Fig 1a). This is followed by a subsequent expansion of BRSK1 and 2 sequences that coincides with the appearance of vertebrates (Fig 3c). Sequence alignment of BRSK catalytic domains from a diverse array of organisms, including the ancestral paralog and invertebrate specific proto-BRSK1, confirmed general sequence similarity and tight conservation of T-loop and HRD proximal Cys 'pairs' (Fig 3d). Interestingly, all BRSK domains also possess a Cys residue in the N-terminal β2-β3 loop ($C54^{BRSK1}$/ $C42^{BRSK2}$), and BRSK2 contains an additional residue at this site, $C39^{BRSK2}$ (Fig 3d). The diversification of BRSKs from AMPKs also correlates with an increase in the total number of Cys residues in the kinase domain (Supp Fig 1a). Analysis of 2805 ARK-related sequences confirmed significant conservation of the T-loop + 2 and HRD -7 Cys, which were found respectively in ~18 % and ~10 % of ePKs across diverse eukaryotic species (Fig 3e). These Cys residues were invariant in vertebrate BRSK sequences, as were the BRSK specific CPE and HRD -1 Cys residues (Fig 3e). Unsurprisingly, substitution of the APE Ala (PKA position 206, found in ~65 % of ePKs) with a Cys is extremely uncommon (~1 %) in nearly all protein kinases, given the critical role of this motif in stabilizing the C-lobe and substrate interactions (Supp Fig 1b). The distribution of amino acids at HRD -1 position is much more variable in ePKs, with Ile and Val being most commonly conserved (~36 and 30 % respectively) and a Cys appearing with similar low frequency (~ 2% (Supp Fig 1b). The high degree of conservation observed for these Cys residues within vertebrate BRSKs indicates that they play critical functional or structural roles in

these kinases (Fig 3e). This further suggests that diversification of the BRSKs in metazoans correlated with the accumulation of close proximity Cys 'pairs' with the potential to form regulatory disulfide bonds.

**Cysteine residues within the kinase domain fine-tune BRSK activity**

To assess the role of BRSK domain Cys residues in modulating catalytic activity, we expressed and purified wild-type (WT) and Cys-to-Ala variants of the BRSK1 and 2 kinase domains in *E. coli*. These Cys-to-Ala variants included T-loop +2 Cys mutants (C191A$^{BRSK1}$ and C176A$^{BRSK2}$), and T-loop CPE mutants (C198A$^{BRSK1}$ and C183A$^{BRSK2}$), expressed either in a WT or mutant T-loop +2 Cys background (C191/198A$^{BRSK1}$ and C176/183A$^{BRSK2}$). We also generated double mutants of the Cys residues upstream of the HRD motif (C147/153A$^{BRSK1}$ and BRSK2 C132/138A$^{BRSK2}$), and the unique N-terminal Cys pair in BRSK2 (C39/42A$^{BRSK2}$). All recombinant BRSK proteins were expressed in *E. coli* and purified without DTT. Crucially, we were able to detect intramolecular disulfide bonds (C191$^{BRSK1}$ - C198$^{BRSK1}$ and C176$^{BRSK2}$ - C183$^{BRSK2}$) in the WT proteins by LC-MS/MS (Supp Fig 2). Interestingly, we could only identify an HRD proximal disulfide bond (C147$^{BRSK1}$ - C153$^{BRSK1}$) in BRSK1 under these specific experimental conditions (Supp Fig 2). We next probed for mixed disulfide formation in the presence of glutathione, using an antibody that recognizes glutathionylated proteins. We detected robust glutathionylation of both BRSK1 and BRSK2 in the presence of either reduced (GSH) or oxidized (GSSG) glutathione, and the signal strength inversely correlated with the presence of DTT (Supp Fig 3a). Of note, all of the BRSK Cys-to-Ala mutants studied here could be readily glutathionylated, which supports the existence of multiple reactive Cys residues within the kinase domains of BRSK1 and 2. To detect alterations in redox regulation, all BRSK proteins were first activated by incubation with LKB1, and T-loop phosphorylation was confirmed by immunoblotting (Supp Fig 3b). The active BRSK1/2 kinases were then assayed using the specific AMARA peptide in the presence or absence of fixed concentrations of DTT. In agreement with our previous findings with full-length BRSKs, DTT was strongly activating for WT variants of both kinases, and this effect was severely blunted for the T-loop +2 Cys-Ala mutants, which exhibited lower basal rates of peptide phosphorylation. This is entirely consistent with

observations for Cys-based mutants of analogous residues in other Ser/Thr kinases (Byrne et al. 2020) (Fig 4a and b). Of note, despite sharing ~95% sequence identity within their kinase domain, LKB1-activated BRSK2 had greater catalytic activity compared to BRSK1 (Fig 4b compared to a). Perhaps unsurprisingly, given their distant location on an N-lobe loop, mutation of the BRSK2 exclusive $C39^{BRSK2}$ and $C42^{BRSK2}$ residues had limited effect on the activity of BRSK2 (Fig 4b). However, tandem mutation of the HRD proximal Cys residues resulted in pronounced abrogation of kinase activity, regardless of assay conditions for both kinases (Fig 4a and b). Given the near absolute conservation of the HRD -7 Cys in the ARK family of protein kinases, it is possible that this residue ($C147^{BRSK1}$ and $C132^{BRSK2}$) is functionally important for catalytic activity in some yet unidentified capacity. Interestingly, mutation of the CPE motif Cys (T-loop +9 Cys), and *de facto* restoration of the canonical APE motif, were insufficient to blunt DTT-dependent activation of either kinase. Moreover, this mutation, which would eliminate $C191^{BRSK1}$ - $C198^{BRSK1}$ and $C176^{BRSK2}$ - $C183^{BRSK2}$ disulfide bonds, increased basal (non-DTT stimulated) catalytic activity by 1.5-2-fold for both kinases. WT forms of BRSK2, and in particular BRSK1, were strongly inhibited by oxidative conditions, even when assays were preceded by DTT-dependent activation (Fig 4c and d). Unsurprisingly, the low levels of detectable $C191A^{BRSK1}$ and $C176A^{BRSK2}$ activity that could be detected following stimulation by DTT were completely abolished following the addition of $H_2O_2$. In contrast, CPE mutants ($C198A^{BRSK1}$ and $C183A^{BRSK2}$) were sharply activated by DTT but still exhibited further oxidative inhibition (Fig 4c and d), although to a lesser extent than their WT counterparts, particularly in the case of BRSK1.

To ensure that the observed variations in activity between variants of BRSK1/2 were not a consequence of structural impairment, we also performed differential scanning fluorometry (DSF) to assess protein folding and stability. Incubation of WT BRSK1 and 2 with DTT had no measurable effect on the thermal stability of either protein, suggesting that chemical disruption of pre-formed disulfide bonds had a minimal detectable impact on protein stability, despite greatly increasing kinase activity (Supp Fig 3c). These assays also revealed only minor perturbations in protein thermal stability due to the incorporation of specified Cys-to-Ala mutants. Interestingly, we observed a consistent decrease in $T_m$ values for $C147/153A^{BRSK1}$ and $C132/138A^{BRSK2}$ ($\Delta T_m$ ~ -2), suggesting a

modest decrease in protein stability, and increased $T_m$ values for CPE mutants (C198A$^{BRSK1}$ and C183A$^{BRSK2}$; $\Delta T_m$ ~ +3) (Supp Fig 3d).

## Cellular analysis of BRSK Cys-based regulation

We next evaluated the relative contributions of the conserved T-loop Cys residues to BRSK redox sensitivity in a cellular context using our EGFP-Tau HEK-293T co-expression system and full length BRSKs. Mirroring our peptide-based kinase assays, loss of the T-loop +2 Cys residue evoked marked abrogation of BRSK-dependent Tau phosphorylation **(**Fig 5a and 5b**).** In contrast, mutation of the CPE Cys to an alanine consistently increased overall Tau phosphorylation (~1.5 and ~1.2 fold increase relative to WT BRSK1 and BRSK2 respectively, Fig 5). Interestingly, the CPE mutations preserved BRSK redox sensitivity in cells treated with hydrogen peroxide, and inclusion of GSH was sufficient to restore BRSK-dependent pTau signals. Finally, we extended our analysis to consider the BRSK1 and 2 HRD motif proximal cysteines, and the BRSK2 exclusive C39/C42 pair. As predicted, Tau phosphorylation by BRSK2 C39/42A (which closely matched the activity profile of WT BRSK2 in our *in vitro* kinase assays (Fig 4)) was comparable to that observed for WT (but still less than hyper-active BRSK2 C183A) and was also similarly inhibited by the presence of $H_2O_2$ (Supp Fig 3e). Using the AMARA peptide as a substrate, we previously demonstrated that BRSK1 C147/153A and BRSK2 C132/138A were catalytically compromised (in a manner resembling the respective T-loop + 2 Cys-Ala mutants (Fig 4)). It is consistent that BRSK2 C132/138A was unable to increase pTau signal above background levels (Sup Fig 3e). Finally, we were unable to detect BRSK1 C147/153A protein expression in transfected cell lysates, which may indicate a loss of stability for this protein.

## Cysteine modifications alter critical structural interactions required for kinase allosteric regulation

We next sought to investigate the structural basis for redox-dependent regulation of BRSK activity using molecular modeling and molecular dynamics (MD) simulations. Our *in vitro* analysis established that oxidative conditions inhibit the active, T-loop phosphorylated form of BRSKs, and so our simulations were performed on an active

conformation of BRSK2 generated using AlphaFold2 (see methods). Cysteine residues can undergo both reversible (sulfenic) and irreversible (sulfonic) oxidation, and so sulfenic acid or sulfonic acid forms of Cys were incorporated at the C176$^{BRSK2}$ and C183$^{BRSK2}$ positions. We also modelled the impact of a non-redox active Ala at these sites.

The T+2 C176$^{BRSK2}$ is in close proximity to threonine T174$^{BRSK2}$, phosphorylation of which stabilizes the kinase domain in an active conformation through salt bridge interactions with charged residues in the catalytic loop (Fig 6a). In particular, R140$^{BRSK2}$ in the canonical HRD motif coordinates with the phosphate group of pT174$^{BRSK2}$ (Nolen, Taylor, and Ghosh 2004). Simulations demonstrate that the R140$^{BRSK2}$-pT174$^{BRSK2}$ salt bridge is preserved across the entire MD simulation, as demonstrated by the contact map (Fig 6b). In the C176Ala$^{BRSK2}$ simulations, the coordination between R140$^{BRSK2}$ and pT174$^{BRSK2}$ is partially attenuated due to an increase in the flexibility of pT174$^{BRSK2}$ (Fig 6c). This predicted increase in flexibility may explain the loss of BRSK2 catalytic activity for C176A$^{BRSK2}$ mutant (Fig 4). However, oxidative modification of C176$^{BRSK2}$ did not result in a significant disruption of the salt bridge interaction (Fig 6d/e). As such, it is unclear at this stage precisely how oxidation of the T+2 Cys exerts is regulatory effect on BRSK2 kinase activity.

In contrast to C176$^{BRSK2}$, C183$^{BRSK2}$ within the CPE motif is buried in the C-terminal lobe of the kinase domain, and the SH group of C183$^{BRSK2}$ is pointed toward a canonical salt bridge that forms between the glutamate (E185$^{BRSK2}$) in the APE/CPE motif and R259$^{BRSK2}$ in the I-helix (Fig 6f). The E185-R259 salt bridge is a eukaryotic protein kinase (EPK)-specific interaction that is critical for maintaining the EPK fold and for allosterically coupling the T-Loop to distal substrate binding and regulatory sites (Yang et al. 2012; Oruganty and Kannan 2012). The selective conservation of Cys in place of Ala in the APE motif represents an interesting divergence of BRSKs from other ARK family kinases (Fig 3e, Supp fig 1). When C183$^{BRSK2}$ is in a reduced form or mutated to an alanine, the E185-R259 is maintained throughout the MD simulation (Fig 6g/i) Remarkably, in simulations incorporating oxidative modification of C183$^{BRSK2}$ we observed the immediate breaking of the E185-R259 salt bridge, and this contact remains broken throughout the simulation (Fig 6h/j). Oxidation of C183$^{BRSK2}$ to either

sulfenic or sulfonic acid rewires this salt bridge, with $R259^{BRSK2}$ exclusively interacting with the oxidized $C183^{BRSK2}$ while $E185^{BRSK2}$ pivots outward and becomes more solvent-exposed. Thus, oxidized $C183^{BRSK2}$ mediated disruption of E185-R259 $^{BRSK2}$ salt bridge represents a unique inactive state in BRSKs which breaks the allosteric network that allows cross-communication between the T-loop and the C-Lobe.

Surprisingly, simulations incorporating intramolecular disulfide bonds identified in MS/MS experiments did not indicate any major changes in dynamics resulting from either the Cys132-138 or the Cys176-183 disulfide bond formation. Most of the fluctuations in these simulations were confined to the G-Loop and β3-αC loop, which are distal from the disulfide bonds (Supp. Fig 4)

**Recombinant BRSK proteins form limited protein dimers**

Several ARK family members form disulfide bond-dependent dimers (Nayak et al. 2006; Marx et al. 2010; Cao et al. 2013). To evaluate the formation of intermolecular disulfides, we subjected purified kinase domains of BRSK1 and 2 isolated from *E. coli* to non-reducing SDS-PAGE, followed by western blotting to probe for higher order BRSK structures (Fig 7). This revealed multiple species of each kinases possessing drastically decreased electrophoretic mobility compared to the major BRSK1/2 monomer bands. These species increased in abundance in the presence of $H_2O_2$ and were absent with DTT. Of particular significance was the appearance of a prominent oxidation-dependent species at ~70 kDa, the approximate molecular weight of a BRSK dimer. All the higher molecular weight species resolved into a single monomer band after reducing (+DTT) SDS-PAGE, which strongly implicates disulfide bond-dependent oligomerization. Curiously, mutation of the T+2 Cys had no discernable effect on the formation of BRSK oligomers, although this is consistent with our previous observation of multiple reactive Cys residues in BRSKs that may be capable of forming a broad variety of intermolecular disulfide bonds. However, it is noteworthy that even in the presence of peroxide, the majority of the BRSK1 and 2 proteins existed as a monomeric species, which suggests that oligomerization is unlikely to be the primary driver of oxidative inhibition that we detect in kinase-based peptide assays.

Using SEC-MALS, we confirmed that BRSK1 and 2 (purified in the absence of DTT) were near-uniformly monomeric in solution, but possessed the potential to self-

649 associate and form dimers. The molar mass points across the monomer peak indicates
650 a high degree of homogeneity (weight-average molar mass $M_w$ = ~42 kDa ± 0.99 % and
651 ~43 kDa ± 0.25 %, respectively Sup Fig 4a and b). Interestingly, the BRSK2 spectra
652 included a high molecular weight shoulder of an approximate dimer size ($M_w$ = ~75 kDa
653 ± 2.1 %) that exhibited non-uniform molar mass points indicative of a heterogenous
654 population (likely as a consequence of poor separation between the two peaks and
655 higher order oligomers)). Although we have searched for BRSK1/2 inter-molecular
656 disulfide bonds in our LC-MS/MS data in an attempt to characterize the mechanism of
657 dimer formation, we were unable to identify any inter-molecular linked peptides. This is
658 likely due to the extremely low abundance of these dimeric species in this sample (thus
659 yielding a very small proportion of inter-linked tryptic peptides) and/or because inter-
660 molecular disulfide linked tryptic peptides are too large for identification using this
661 analytical pipeline. Collectively these findings confirm that the isolated kinase domains
662 of both BRSKs primarily occupy a largely monomeric conformation and can form limited
663 higher order redox-sensitive oligomers via covalent S-S bonds *in vitro*. However,
664 although reversible oxidation-based inactivation of BRSK1 and 2 is apparent in full-
665 length BRSK1 and 2, it remains to be determined to what extent multimerization
666 modulates BRSK catalytic activity (Fig 8) or how these mechanisms might contribute to
667 signaling-based interactions in cells.
668

## Discussion

Redox regulation of kinases and other signaling molecules is a rapidly expanding field of research, which has extended far beyond the early observations of oxidative inhibition in protein tyrosine phosphatases (Brandes, Schmitt, and Jakob 2009). More recent enquiries have provided strong evidence for direct regulative oxidative modification of Met and Cys residues across divergent protein kinase families, providing temporal and spatial control of their catalytic outputs (Corcoran and Cotter 2013; Truong and Carroll 2013; Jarvis, Hughes, and Ledgerwood 2012). However, despite the prevalence of this regulatory mechanism, the structural basis for how redox-active cysteines contribute to allosteric control of catalytic activity is largely unknown. In this study, we demonstrate, for the first time, that two T-loop +2 Cys-containing members of the ARK family, BRSK1 and 2, are reversibly inactivated by oxidative-dependent mechanisms *in vitro* and in human cells. Moreover, we uncover a multifaceted redox-activity profile for human BRSKs, involving functional Cys-pairs that are conserved within the catalytic domains of these understudied enzymes (Fig 8). In contrast to kinases such as Aurora A, where a single Cys residue is the dominant driver of redox-sensitivity (Byrne et al. 2020; Tsuchiya et al. 2020), BRSK1 and 2 possess multiple sulfenylation-prone Cys residues (validated by their susceptibility to glutathionylation and ability to form intramolecular disulfide bonds (Fig 2 and Supp Fig 3)) that leads to direct modification of catalytic output. The close proximity of these Cys 'pairs' permits the formation of two intramolecular disulfide bonds: the first forming between two HRD-motif proximal sites, and the second bridging the conserved T-loop + 2 and unique 'CPE' motif Cys residues (Fig 2). We propose a model where disulfide bond formation can impose a steric block on kinase activity whilst structural perturbations, likely emanating from sulfenylation of conserved BRSK family Cys residues within critical kinase regulatory motifs, provides an additional layer of tunable regulation (Fig 8). Importantly, MD simulations suggest that CPE Cys oxidation would cause disruption of the CPE-I-helix salt bridge, critical for maintaining the EPK fold and allosteric communication within the kinase domain. Mechanistically, oxidation of this Cys would hijack the I-helix Arg, disrupting the allosteric network with the CPE Glu, which concomitantly becomes more solvent-exposed. This insight provides a new

understanding of BRSK regulation at the structural level and has potential implications in cellular signaling and diseases that warrant further investigation. Validation of these reversibly oxidized Cys species is also of interest relevance as this may implicate a mechanistic role for ROS sensing in the largely obscure BRSK signaling pathways that operate in different cell types, including those that impact on canonical redox pathways that lead to NRF2 inactivation in cells (Tamir et al. 2020).

**Multilayered redox regulation of BRSKs**

The close proximity of Cys residues to critical regulatory elements within the T-Loop (Beenstock, Mooshayef, and Engelberg 2016; Pearce, Komander, and Alessi 2010) is likely to be a strategic evolutionary adaptation to permit ROS-based sensing and regulated signaling in protein kinases. To attain 'full' activity, almost all ePKs need to be phosphorylated on a T-Loop site, either in a self-activating manner (autophosphorylation) or by an upstream kinase(s). This major regulatory step results in a conformational reorganization, leading to the stabilization of an appropriate active conformation to enable efficient catalytic transfer of phosphate to a protein substrate. Although T-Loop phosphorylation is a critical and highly controlled process necessary to convert kinases from inactive to active conformations, phosphorylation-independent activation mechanism that bypass, or function as an accessory to this step have also been described, such as allosteric activation of Aurora A by TPX2 (Eyers et al. 2003, Bayliss et al. 2003), or activation of CAMKs by CaM (Rellos et al. 2010). Moreover, kinase activity can be further fine-tuned by a mechanistically diverse array of supplementary interactions and modifications, including ROS-derived Cys adducts. ARK family kinases, such as BRSK1 and 2, are primed by phosphorylation in the T-loop of a single Thr residue by the master regulator. LKB1. However, our findings suggest that oxidation (or reduction) of key reactive Cys residues in the kinase domains of BRSK1 +2 might provide a 'dominant' regulatory oversight of enzyme output whose function in cells is likely controlled by subcellular compartmentalization and/or partner protein interactions.

The ARK family of protein kinases, consisting of 14 members (including AMPKα) share related structural architecture and sequence homology, including a conserved T-loop +

2 Cys residue distal to the activating site of phosphorylation. In this context, it is noteworthy that several ARKs, including AMPK itself, are already known to be regulated by redox modification in some capacity, and this has been attributed in large part to the T+2 Cys residue (Byrne et al. 2020). As observed for several other Ser/Thr kinases, amino acid substitutions at the T+2 Cys position are poorly tolerated in BRSKs (Fig 4 and 5), resulting in loss of activity, and confirming an indirect functional role of this Cys residue in catalysis. Curiously, across diverse eukaryotic species, an additional Cys residue (HRD -7) is nearly ubiquitously co-conserved alongside the T-loop Cys in all ARKs, with the notable exception of MELK kinases (Fig 3). The close-proximity of the HRD-7 Cys to the canonical HRD motif is predicted to provide an additional layer of regulation in ARK family kinases. Indeed, the substitution of HRD-7 Cys with alanine is highly detrimental to kinase activity (but not stability) of BRSK1 and 2 (Fig 4 and Supp Fig 3d), which is consistent with a central role in maintaining an active conformation. Moreover, the equivalent residue of AMPK, Cys 130, has previously been linked to the redox-activity profile of this energy-monitoring kinase (Shao et al. 2014). Additionally, several ARK family members form disulfide bond-dependent homo- and hetero dimers with other proteins (Nayak et al. 2006; Marx et al. 2010; Cao et al. 2013). The crystal structures of ARK family members MELK and MARK2 members demonstrate asymmetric dimers, covalently linked by a disulfide bridge formed between T-loop + 2 Cys residues, and all demonstrate a similar mode of interaction consistent with a symetry mate that can also be observed in the crystal structure of BRSK2 (Fig 8b), (Marx et al. 2010; Marx et al. 2006; Murphy et al. 2007; Cao et al. 2013)).

**BRSK-specific adaptations relevant to Cys-based signaling?**

BRSKs are differentiated from other ARKs (and ePKs) by being further augmented with two ‘BRSK-specific’ Cys residues at the HRD -1 and T-loop +9 positions, in close proximity to the co-conserved HRD -7 and T-loop +2 Cys residues, respectively. The identification of a T-loop + 9 Cys in BRSKs is particularly intriguing, as this replaces the near invariant Ala residue of the APE motif found in the majority of human protein kinases, creating a new ‘CPE’ motif. These adjacent cysteine pairs are also sufficiently contiguous to support formation of intramolecular disulfide bonds that we can readily

identify by MS, and which we predict impose a stable inactive conformation on the kinase. This observation can likely explain the near obligate requirement of both kinases for reducing agents to stimulate catalysis, in a manner reminiscent of AKT and MELK; two protein kinases that can be released from an inactive-oxidized state by the chemical reduction of auto-inhibitory intramolecular disulfide bonds (Murata et al. 2003; Huang et al. 2003; Byrne et al. 2020; Beullens et al. 2005). Furthermore, deletion of the more distal T-loop Cys residue in the CPE motif is sufficient to partially blunt BRSK1 and 2 auto-inhibition, which we partially accredit to the elimination of this covalent bond. In this regard, it is of note that our MD simulations also suggest that the CPE Cys may have several functional roles, as the oxidized form is also capable of directly disrupting the CPE-I-helix salt bridge. Interestingly, although restoration of a *de facto* APE motif was highly activating (relative to WT BRSK proteins), it was ineffective at suppressing further oxidative inhibition in the presence of peroxide. This signifies that other redox-sensitive cysteines, and notably the T-loop +2 Cys, may co-ordinate the catalytic response of BRSKs to ROS. Through comparative evolutionary analysis, we identified that ~1.4 % of all ePKs (including AKT and MELK) possess spatially organized cysteines capable of disulfide bridging the DFG + 2 and T-loop + 2 positions (Byrne et al. 2020; Cao et al. 2013)(Huang et al. 2003). Notably, although MELK lacks the characteristic HRD -7 Cys that is a hallmark of ARKs, it has accumulated 'compensatory' activation loop Cys residues capable of forming an array of interchangeable disulfide bonds (*in vitro*) between the aforementioned DFG +2 position and an unusual tandem Cys arrangement at the T-loop +1 and + 2 positions (Beullens et al. 2005). Furthermore, a broad analysis of potential disulfide pairs within the catalytic domain of all human protein kinases reveals 273 unique Cys pairs across 138 kinases with cysteine pairs within 10 Å of each other in the AlphaFold database (Supp. File 1). Although the potential for these pairs to form reversible disulfide bonds needs to be established experimentally, the prevalence of these pairs across the kinome suggests that conformational control of kinase activity through reversible disulfide bonds may be a prevalent mechanism of kinome regulation. In this study, we report a diverse intramolecular disulfide network in BRSK1 and 2 that we predict serves as an intrinsic reversible switch to modify BRSK-based partner interactions and signaling. When considering the dominant regulative role of the T-loop

T+2 Cys, it is tempting to speculate that formation of such intramolecular disulfides bonds with adjacent cysteines may be a protective physiological adaptation to prevent formation of deleterious hyper-oxidized species and enable rapid re-activation of the kinase after emergence from oxidative stress conditions by the disulfide reductase system (Krishnan et al. 2011; Barrett et al. 1999; Chen et al. 2008).

The identification and characterization of unique reactive Cys residues within the kinase domains of BRSK1 and 2 reveals sites of covalent-oxidative modification that may also provide an underexploited opportunity to develop targeted therapeutic strategies for BRSK-associated pathologies. Furthermore, mapping the spatial distribution of Cys across the AMPK-related kinase family provides valuable insights into potential redox hotspots that may underpin a tunable modulation of catalytic outputs with wider implications for cellular signaling. As a master regulator of metabolic homeostasis, AMPK activity is central to appropriate redox balance within cells (Ren and Shen 2019; Choi et al. 2001; Hawley et al. 2010; Zmijewski et al. 2010; Hinchy et al. 2018; Auciello et al. 2014; Shao et al. 2014), but until recently evidence of crosstalk between BRSKs and redox signaling has been less clear. However, BRSKs can indirectly modulate the cellular antioxidant response by orchestrating suppression of the transcription factor (and master regulator/sensor of the antioxidant response), NRF2, in an mTOR-dependent manner (Tamir et al. 2020). NRF2 is targeted for proteasomal degradation by its inhibitor partner, KEAP1, and under conditions of elevated ROS, oxidation of sensor Cys residues in KEAP1 allows NRF2 to escape ubiquitination and induce transcription of the antioxidant machinery (Baird and Yamamoto 2020). Our discovery of redox regulation in BRSKs suggests that it may be part of a multi-protein Cys-based ‘relay’ network of ROS sensitive effectors upstream of NRF2, potentially constituting a new oxidative stress signaling mechanism. Uncoupling the specific role of BRSKs in this pathway will be critical in illuminating BRSK1 and 2 physiology and their roles in neuronal function and disease and may simultaneously provide an explanation for the appearance of two functional BRSK1/2 genes in vertebrates.

## Author Contributions

N.K. and P.A.E. conceptualization; G.N.B., D.P.B., C.E.E., P.A.E., and N.K. methodology; G.N.B., D.P.B., S.S., L.A.D., S.O.O., S.K., A.V. and W.Y. investigation; G.B.D., D.P.B., L.A.D. and S.O.O. data curation; G.N.B., D.P.B., S.S., L.A.D., S.O.O., S.K., A.V. and W.Y. formal analysis; G.N.B., D.P.B., S.S., L.A.D., S.O.O., S.K., A.V. and W.Y. validation; G.N.B., D.P.B., P.A.E., and N.K. writing – original draft; G.N.B., D.P.B., S.S., L.A.D., S.O.O., S.K., A.V., W.Y. C.E.E., P.A.E. and N.K. writing – review and editing; A.V., G.W., D.P.B., B.O., and S.S. visualization; P.A.E., C.E.E. and N.K. supervision; C.E.E., P.A.E., and N.K. funding acquisition.

## Funding and additional information

Funding from N.K. (grant no: R35 GM139656) is acknowledged. P.A.E. acknowledges funding from University of Liverpool BBSRC MRC/IAA awards. A.V. acknowledges funding from ARCS Foundation. D.P.B, L.A.D., S.O.O., P.A.E. and C.E.E. also acknowledge BBSRC grants BB/S018514/1, BB/N021703/1, BB/X002780/1 and North West Cancer Research (NWCR) grant CR1208. The content is solely the responsibility of the authors and does not necessarily represent the official views of the National Institutes of Health.

## Data Availability

All data generated in this study are included within the manuscript. All mass spectrometry data has been deposited at the ProteomeXchange Consortium (http://proteomecentral.proteomexchange.org) via the PRIDE partner repository with the dataset identifiers PXD044990. Source data are provided for each figure. MD simulations and associated data may be accessed from https://www.dropbox.com/sh/xtiwpjgyzxy1oz0/AACK6dS3ypzYXDih3wgKp9bla?dl=0.

## Competing Interest Statement

The authors claim no competing interest.

## References

Alessi, D. R., K. Sakamoto, and J. R. Bayascas. 2006. 'LKB1-dependent signaling pathways', Annu Rev Biochem, 75: 137-63.

Auciello, F. R., F. A. Ross, N. Ikematsu, and D. G. Hardie. 2014. 'Oxidative stress activates AMPK in cultured cells primarily by increasing cellular AMP and/or ADP', Febs Letters, 588: 3361-6.

Baird, L., and M. Yamamoto. 2020. 'The Molecular Mechanisms Regulating the KEAP1-NRF2 Pathway', Mol Cell Biol, 40.

Barrett, W. C., J. P. DeGnore, S. Konig, H. M. Fales, Y. F. Keng, Z. Y. Zhang, M. B. Yim, and P. B. Chock. 1999. 'Regulation of PTP1B via glutathionylation of the active site cysteine 215', Biochemistry, 38: 6699-705.

Bayliss, R., T. Sardon, I. Vernos, and E. Conti. 2003. 'Structural basis of Aurora-A activation by TPX2 at the mitotic spindle', Mol Cell, 12: 851-62.

Beenstock, J., N. Mooshayef, and D. Engelberg. 2016. 'How Do Protein Kinases Take a Selfie (Autophosphorylate)?', Trends Biochem Sci, 41: 938-53.

Beullens, M., S. Vancauwenbergh, N. Morrice, R. Derua, H. Ceulemans, E. Waelkens, and M. Bollen. 2005. 'Substrate specificity and activity regulation of protein kinase MELK', J Biol Chem, 280: 40003-11.

Brandes, N., S. Schmitt, and U. Jakob. 2009. 'Thiol-based redox switches in eukaryotic proteins', Antioxid Redox Signal, 11: 997-1014.

Bright, N. J., D. Carling, and C. Thornton. 2008. 'Investigating the regulation of brain-specific kinases 1 and 2 by phosphorylation', J Biol Chem, 283: 14946-54.

Bright, N. J., C. Thornton, and D. Carling. 2009. 'The regulation and function of mammalian AMPK-related kinases', Acta Physiol (Oxf), 196: 15-26.

Brooks, B. R., C. L. Brooks, 3rd, A. D. Mackerell, Jr., L. Nilsson, R. J. Petrella, B. Roux, Y. Won, G. Archontis, C. Bartels, S. Boresch, A. Caflisch, L. Caves, Q. Cui, A. R. Dinner, M. Feig, S. Fischer, J. Gao, M. Hodoscek, W. Im, K. Kuczera, T. Lazaridis, J. Ma, V. Ovchinnikov, E. Paci, R. W. Pastor, C. B. Post, J. Z. Pu, M. Schaefer, B. Tidor, R. M. Venable, H. L. Woodcock, X. Wu, W. Yang, D. M. York, and M. Karplus. 2009. 'CHARMM: the biomolecular simulation program', Journal of Computational Chemistry, 30: 1545-614.

Byrne, D. P., S. Shrestha, M. Galler, M. Cao, L. A. Daly, A. E. Campbell, C. E. Eyers, E. A. Veal, N. Kannan, and P. A. Eyers. 2020. 'Aurora A regulation by reversible cysteine oxidation reveals evolutionarily conserved redox control of Ser/Thr protein kinase activity', Sci Signal, 13.

Byrne, D. P., M. Vonderach, S. Ferries, P. J. Brownridge, C. E. Eyers, and P. A. Eyers. 2016. 'cAMP-dependent protein kinase (PKA) complexes probed by complementary differential scanning fluorimetry and ion mobility-mass spectrometry', Biochem J, 473: 3159-75.

889 Cao, L. S., J. Wang, Y. Chen, H. Deng, Z. X. Wang, and J. W. Wu. 2013. 'Structural
890 basis for the regulation of maternal embryonic leucine zipper kinase', PLoS One, 8:
891 e70031.

892 Cao, M., A. M. Day, M. Galler, H. R. Latimer, D. P. Byrne, T. W. Foy, E. Dwyer, E.
893 Bennett, J. Palmer, B. A. Morgan, P. A. Eyers, and E. A. Veal. 2023. 'A peroxiredoxin-
894 P38 MAPK scaffold increases MAPK activity by MAP3K-independent mechanisms', Mol
895 Cell.

896 Chen, Y. Y., H. M. Chu, K. T. Pan, C. H. Teng, D. L. Wang, A. H. Wang, K. H. Khoo,
897 and T. C. Meng. 2008. 'Cysteine S-nitrosylation protects protein-tyrosine phosphatase
898 1B against oxidation-induced permanent inactivation', J Biol Chem, 283: 35265-72.

899 Choi, S. L., S. J. Kim, K. T. Lee, J. Kim, J. Mu, M. J. Birnbaum, S. Soo Kim, and J. Ha.
900 2001. 'The regulation of AMP-activated protein kinase by H(2)O(2)', Biochem Biophys
901 Res Commun, 287: 92-7.

902 Corcoran, A., and T. G. Cotter. 2013. 'Redox regulation of protein kinases', Febs
903 Journal, 280: 1944-65.

904 Daly, L. A., P. J. Brownridge, M. Batie, S. Rocha, V. See, and C. E. Eyers. 2021.
905 'Oxygen-dependent changes in binding partners and post-translational modifications
906 regulate the abundance and activity of HIF-1alpha/2alpha', Sci Signal, 14.

907 Daly, Leonard A, Dominic P Byrne, Simon Perkins, Philip J Brownridge, Euan
908 McDonnell, Andrew R Jones, Patrick A Eyers, and Claire E Eyers. 2023. 'A bespoke
909 analytical workflow for the confident identification of sulfopeptides and their
910 discrimination from phosphopeptides', bioRxiv: 2023.07. 15.549150.

911 Deng, J., Y. Wang, M. Hu, J. Lin, Q. Li, C. Liu, and X. Xu. 2022. 'Deleterious Variation in
912 BR Serine/Threonine Kinase 2 Classified a Subtype of Autism', Front Mol Neurosci, 15:
913 904935.

914 Engh, R. A., and D. Bossemeyer. 2001. 'The protein kinase activity modulation sites:
915 mechanisms for cellular regulation - targets for therapeutic intervention', Adv Enzyme
916 Regul, 41: 121-49.

917 Eyers, P. A., E. Erikson, L. G. Chen, and J. L. Maller. 2003. 'A novel mechanism for
918 activation of the protein kinase Aurora A', Curr Biol, 13: 691-7.

919 Faezov, Bulat, and Jr. Roland L. Dunbrack. 2023. 'AlphaFold2 models of the active form
920 of all 437 catalytically-competent typical human kinase domains', bioRxiv:
921 2023.07.21.550125.

922 Ferries, S., S. Perkins, P. J. Brownridge, A. Campbell, P. A. Eyers, A. R. Jones, and C.
923 E. Eyers. 2017. 'Evaluation of Parameters for Confident Phosphorylation Site
924 Localization Using an Orbitrap Fusion Tribrid Mass Spectrometer', J Proteome Res, 16:
925 3448-59.

926 Fomenko, D. E., S. M. Marino, and V. N. Gladyshev. 2008. 'Functional diversity of
927 cysteine residues in proteins and unique features of catalytic redox-active cysteines in
928 thiol oxidoreductases', Mol Cells, 26: 228-35.

929 Forman, H. J., M. J. Davies, A. C. Kramer, G. Miotto, M. Zaccarin, H. Zhang, and F.
930 Ursini. 2017. 'Protein cysteine oxidation in redox signaling: Caveats on sulfenic acid
931 detection and quantification', Arch Biochem Biophys, 617: 26-37.

932 Foulkes, D. M., D. P. Byrne, W. Yeung, S. Shrestha, F. P. Bailey, S. Ferries, C. E.
933 Eyers, K. Keeshan, C. Wells, D. H. Drewry, W. J. Zuercher, N. Kannan, and P. A.
934 Eyers. 2018. 'Covalent inhibitors of EGFR family protein kinases induce degradation of
935 human Tribbles 2 (TRIB2) pseudokinase in cancer cells', Sci Signal, 11.

936 Garrido Ruiz, D., A. Sandoval-Perez, A. V. Rangarajan, E. L. Gunderson, and M. P.
937 Jacobson. 2022. 'Cysteine Oxidation in Proteins: Structure, Biophysics, and Simulation',
938 Biochemistry, 61: 2165-76.

939 Gupta, V., and K. S. Carroll. 2014. 'Sulfenic acid chemistry, detection and cellular
940 lifetime', Biochim Biophys Acta, 1840: 847-75.

941 Hawley, S. A., F. A. Ross, C. Chevtzoff, K. A. Green, A. Evans, S. Fogarty, M. C.
942 Towler, L. J. Brown, O. A. Ogunbayo, A. M. Evans, and D. G. Hardie. 2010. 'Use of cells
943 expressing gamma subunit variants to identify diverse mechanisms of AMPK activation',
944 Cell Metab, 11: 554-65.

945 Heppner, D. E., Y. M. W. Janssen-Heininger, and A. van der Vliet. 2017. 'The role of
946 sulfenic acids in cellular redox signaling: Reconciling chemical kinetics and molecular
947 detection strategies', Arch Biochem Biophys, 616: 40-46.

948 Hinchy, E. C., A. V. Gruszczyk, R. Willows, N. Navaratnam, A. R. Hall, G. Bates, T. P.
949 Bright, T. Krieg, D. Carling, and M. P. Murphy. 2018. 'Mitochondria-derived ROS
950 activate AMP-activated protein kinase (AMPK) indirectly', J Biol Chem, 293: 17208-17.

951 Hoang, D. T., O. Chernomor, A. von Haeseler, B. Q. Minh, and L. S. Vinh. 2018.
952 'UFBoot2: Improving the Ultrafast Bootstrap Approximation', Molecular Biology and
953 Evolution, 35: 518-22.

954 Huang, X., M. Begley, K. A. Morgenstern, Y. Gu, P. Rose, H. Zhao, and X. Zhu. 2003.
955 'Crystal structure of an inactive Akt2 kinase domain', Structure, 11: 21-30.

956 Huerta-Cepas, J., F. Serra, and P. Bork. 2016. 'ETE 3: Reconstruction, Analysis, and
957 Visualization of Phylogenomic Data', Molecular Biology and Evolution, 33: 1635-8.

958 Humphries, K. M., C. Juliano, and S. S. Taylor. 2002. 'Regulation of cAMP-dependent
959 protein kinase activity by glutathionylation', J Biol Chem, 277: 43505-11.

960 Jarvis, R. M., S. M. Hughes, and E. C. Ledgerwood. 2012. 'Peroxiredoxin 1 functions as
961 a signal peroxidase to receive, transduce, and transmit peroxide signals in mammalian
962 cells', Free Radic Biol Med, 53: 1522-30.

963 Jo, S., X. Cheng, S. M. Islam, L. Huang, H. Rui, A. Zhu, H. S. Lee, Y. Qi, W. Han, K.
964 Vanommeslaeghe, A. D. MacKerell, Jr., B. Roux, and W. Im. 2014. 'CHARMM-GUI PDB
965 manipulator for advanced modeling and simulations of proteins containing nonstandard
966 residues', Adv Protein Chem Struct Biol, 96: 235-65.

967 Jumper, J., R. Evans, A. Pritzel, T. Green, M. Figurnov, O. Ronneberger, K.
968 Tunyasuvunakool, R. Bates, A. Zidek, A. Potapenko, A. Bridgland, C. Meyer, S. A. A.

969 Kohl, A. J. Ballard, A. Cowie, B. Romera-Paredes, S. Nikolov, R. Jain, J. Adler, T. Back,
970 S. Petersen, D. Reiman, E. Clancy, M. Zielinski, M. Steinegger, M. Pacholska, T.
971 Berghammer, S. Bodenstein, D. Silver, O. Vinyals, A. W. Senior, K. Kavukcuoglu, P.
972 Kohli, and D. Hassabis. 2021. 'Highly accurate protein structure prediction with
973 AlphaFold', Nature, 596: 583-89.

974 Kalyaanamoorthy, S., B. Q. Minh, T. K. F. Wong, A. von Haeseler, and L. S. Jermiin.
975 2017. 'ModelFinder: fast model selection for accurate phylogenetic estimates', Nat
976 Methods, 14: 587-89.

977 Kishi, M., Y. A. Pan, J. G. Crump, and J. R. Sanes. 2005. 'Mammalian SAD kinases are
978 required for neuronal polarization', Science, 307: 929-32.

979 Krishnan, N., C. Fu, D. J. Pappin, and N. K. Tonks. 2011. 'H2S-Induced sulfhydration of
980 the phosphatase PTP1B and its role in the endoplasmic reticulum stress response', Sci
981 Signal, 4: ra86.

982 Lee, J., X. Cheng, J. M. Swails, M. S. Yeom, P. K. Eastman, J. A. Lemkul, S. Wei, J.
983 Buckner, J. C. Jeong, Y. Qi, S. Jo, V. S. Pande, D. A. Case, C. L. Brooks, 3rd, A. D.
984 MacKerell, Jr., J. B. Klauda, and W. Im. 2016. 'CHARMM-GUI Input Generator for
985 NAMD, GROMACS, AMBER, OpenMM, and CHARMM/OpenMM Simulations Using the
986 CHARMM36 Additive Force Field', J Chem Theory Comput, 12: 405-13.

987 Lennicke, C., J. Rahn, R. Lichtenfels, L. A. Wessjohann, and B. Seliger. 2015.
988 'Hydrogen peroxide - production, fate and role in redox signaling of tumor cells', Cell
989 Commun Signal, 13: 39.

990 Li, R., M. He, B. Wu, P. Zhang, Q. Zhang, and Y. Chen. 2020. 'SAD-B modulates
991 epileptic seizure by regulating AMPA receptors in patients with temporal lobe epilepsy
992 and in the PTZ-induced epileptic model', Braz J Med Biol Res, 53: e9175.

993 Lizcano, J. M., O. Goransson, R. Toth, M. Deak, N. A. Morrice, J. Boudeau, S. A.
994 Hawley, L. Udd, T. P. Makela, D. G. Hardie, and D. R. Alessi. 2004. 'LKB1 is a master
995 kinase that activates 13 kinases of the AMPK subfamily, including MARK/PAR-1',
996 EMBO J, 23: 833-43.

997 Manning, G., D. B. Whyte, R. Martinez, T. Hunter, and S. Sudarsanam. 2002. 'The
998 protein kinase complement of the human genome', Science, 298: 1912-34.

999 Marx, A., C. Nugoor, J. Muller, S. Panneerselvam, T. Timm, M. Bilang, E. Mylonas, D. I.
1000 Svergun, E. M. Mandelkow, and E. Mandelkow. 2006. 'Structural variations in the
1001 catalytic and ubiquitin-associated domains of microtubule-associated
1002 protein/microtubule affinity regulating kinase (MARK) 1 and MARK2', J Biol Chem, 281:
1003 27586-99.

1004 Marx, A., C. Nugoor, S. Panneerselvam, and E. Mandelkow. 2010. 'Structure and
1005 function of polarity-inducing kinase family MARK/Par-1 within the branch of AMPK/Snf1-
1006 related kinases', FASEB J, 24: 1637-48.

1007 Michaud-Agrawal, N., E. J. Denning, T. B. Woolf, and O. Beckstein. 2011. 'MDAnalysis:
1008 a toolkit for the analysis of molecular dynamics simulations', Journal of Computational
1009 Chemistry, 32: 2319-27.

1010 Minh, B. Q., H. A. Schmidt, O. Chernomor, D. Schrempf, M. D. Woodhams, A. von
1011 Haeseler, and R. Lanfear. 2020. 'IQ-TREE 2: New Models and Efficient Methods for
1012 Phylogenetic Inference in the Genomic Era', Molecular Biology and Evolution, 37: 1530-
1013 34.

1014 Mohanty, S., K. Oruganty, A. Kwon, D. P. Byrne, S. Ferries, Z. Ruan, L. E. Hanold, S.
1015 Katiyar, E. J. Kennedy, P. A. Eyers, and N. Kannan. 2016. 'Hydrophobic Core Variations
1016 Provide a Structural Framework for Tyrosine Kinase Evolution and Functional
1017 Specialization', PLoS Genet, 12: e1005885.

1018 Morshed, Nader, Meelim J Lee, Felicia H Rodriguez, Douglas A Lauffenburger, Diego
1019 Mastroeni, and Forest M White. 2021. 'Quantitative phosphoproteomics uncovers
1020 dysregulated kinase networks in Alzheimer's disease', Nature Aging, 1: 550-65.

1021 Murata, H., Y. Ihara, H. Nakamura, J. Yodoi, K. Sumikawa, and T. Kondo. 2003.
1022 'Glutaredoxin exerts an antiapoptotic effect by regulating the redox state of Akt', J Biol
1023 Chem, 278: 50226-33.

1024 Murphy, J. M., D. M. Korzhnev, D. F. Ceccarelli, D. J. Briant, A. Zarrine-Afsar, F.
1025 Sicheri, L. E. Kay, and T. Pawson. 2007. 'Conformational instability of the MARK3 UBA
1026 domain compromises ubiquitin recognition and promotes interaction with the adjacent
1027 kinase domain', Proc Natl Acad Sci U S A, 104: 14336-41.

1028 Murphy, J. M., Q. Zhang, S. N. Young, M. L. Reese, F. P. Bailey, P. A. Eyers, D.
1029 Ungureanu, H. Hammaren, O. Silvennoinen, L. N. Varghese, K. Chen, A. Tripaydonis,
1030 N. Jura, K. Fukuda, J. Qin, Z. Nimchuk, M. B. Mudgett, S. Elowe, C. L. Gee, L. Liu, R. J.
1031 Daly, G. Manning, J. J. Babon, and I. S. Lucet. 2014. 'A robust methodology to
1032 subclassify pseudokinases based on their nucleotide-binding properties', Biochem J,
1033 457: 323-34.

1034 Nayak, V., K. Zhao, A. Wyce, M. F. Schwartz, W. S. Lo, S. L. Berger, and R.
1035 Marmorstein. 2006. 'Structure and dimerization of the kinase domain from yeast Snf1, a
1036 member of the Snf1/AMPK protein family', Structure, 14: 477-85.

1037 Nakanishi, K., H. Niida, H. Tabata, T. Ito, Y. Hori, M. Hattori, Y. Johmura, C. Yamada, T.
1038 Ueda, K. Takeuchi, K. Yamada, K. Nagata, N. Wakamatsu, M. Kishi, Y. A. Pan, S.
1039 Ugawa, S. Shimada, J. R. Sanes, Y. Higashi, and M. Nakanishi. 2019. 'Isozyme-
1040 Specific Role of SAD-A in Neuronal Migration During Development of Cerebral Cortex',
1041 Cerebral Cortex, 29: 3738-51.

1042 Nayak, V., K. Zhao, A. Wyce, M. F. Schwartz, W. S. Lo, S. L. Berger, and R.
1043 Marmorstein. 2006. 'Structure and dimerization of the kinase domain from yeast Snf1, a
1044 member of the Snf1/AMPK protein family', Structure, 14: 477-85.

1045 Neuwald, A. F. 2009. 'Rapid detection, classification and accurate alignment of up to a
1046 million or more related protein sequences', Bioinformatics, 25: 1869-75.

1047 Nie, J., C. Sun, O. Faruque, G. Ye, J. Li, Q. Liang, Z. Chang, W. Yang, X. Han, and Y.
1048 Shi. 2012. 'Synapses of amphids defective (SAD-A) kinase promotes glucose-
1049 stimulated insulin secretion through activation of p21-activated kinase (PAK1) in
1050 pancreatic beta-Cells', J Biol Chem, 287: 26435-44.

1051 Nolen, B., S. Taylor, and G. Ghosh. 2004. 'Regulation of protein kinases; controlling
1052 activity through activation segment conformation', Mol Cell, 15: 661-75.

1053 Pearce, L. R., D. Komander, and D. R. Alessi. 2010. 'The nuts and bolts of AGC protein
1054 kinases', Nat Rev Mol Cell Biol, 11: 9-22.

1055 Perkins, D. N., D. J. Pappin, D. M. Creasy, and J. S. Cottrell. 1999. 'Probability-based
1056 protein identification by searching sequence databases using mass spectrometry data',
1057 Electrophoresis, 20: 3551-67.

1058 Poole, L. B. 2015. 'The basics of thiols and cysteines in redox biology and chemistry',
1059 Free Radic Biol Med, 80: 148-57.

1060 Rellos, P., A. C. Pike, F. H. Niesen, E. Salah, W. H. Lee, F. von Delft, and S. Knapp.
1061 2010. 'Structure of the CaMKIIdelta/calmodulin complex reveals the molecular
1062 mechanism of CaMKII kinase activation', PLoS Biol, 8: e1000426.

1063 Ren, Y., and H. M. Shen. 2019. 'Critical role of AMPK in redox regulation under glucose
1064 starvation', Redox Biol, 25: 101154.

1065 Rhee, S. G., S. W. Kang, W. Jeong, T. S. Chang, K. S. Yang, and H. A. Woo. 2005.
1066 'Intracellular messenger function of hydrogen peroxide and its regulation by
1067 peroxiredoxins', Curr Opin Cell Biol, 17: 183-9.

1068 Saiyin, H., N. Na, X. Han, Y. Fang, Y. Wu, W. Lou, and X. Yang. 2017. 'BRSK2 induced
1069 by nutrient deprivation promotes Akt activity in pancreatic cancer via downregulation of
1070 mTOR activity', Oncotarget, 8: 44669-81.

1071 Salmeen, A., J. N. Andersen, M. P. Myers, T. C. Meng, J. A. Hinks, N. K. Tonks, and D.
1072 Barford. 2003. 'Redox regulation of protein tyrosine phosphatase 1B involves a
1073 sulphenyl-amide intermediate', Nature, 423: 769-73.

1074 Schieber, M., and N. S. Chandel. 2014. 'ROS function in redox signaling and oxidative
1075 stress', Curr Biol, 24: R453-62.

1076 Schrodinger, LLC. 2015. "The PyMOL Molecular Graphics System, Version 1.8." In.

1077 Shao, D., S. Oka, T. Liu, P. Zhai, T. Ago, S. Sciarretta, H. Li, and J. Sadoshima. 2014.
1078 'A redox-dependent mechanism for regulation of AMPK activation by Thioredoxin1
1079 during energy starvation', Cell Metab, 19: 232-45.

1080 Shirwany, N. A., and M. H. Zou. 2014. 'AMPK: a cellular metabolic and redox sensor. A
1081 minireview', Front Biosci (Landmark Ed), 19: 447-74.

1082 Soylu, I., and S. M. Marino. 2016. 'Cy-preds: An algorithm and a web service for the
1083 analysis and prediction of cysteine reactivity', Proteins, 84: 278-91.

1084 Su, Z., J. G. Burchfield, P. Yang, S. J. Humphrey, G. Yang, D. Francis, S. Yasmin, S. Y.
1085 Shin, D. M. Norris, A. L. Kearney, M. A. Astore, J. Scavuzzo, K. H. Fisher-Wellman, Q.
1086 P. Wang, B. L. Parker, G. G. Neely, F. Vafaee, J. Chiu, R. Yeo, P. J. Hogg, D. J.
1087 Fazakerley, L. K. Nguyen, S. Kuyucak, and D. E. James. 2019. 'Global redox proteome
1088 and phosphoproteome analysis reveals redox switch in Akt', Nat Commun, 10: 5486.

1089 Tamir, T. Y., D. H. Drewry, C. Wells, M. B. Major, and A. D. Axtman. 2020. 'PKIS deep
1090 dive yields a chemical starting point for dark kinases and a cell active BRSK2 inhibitor',
1091 Sci Rep, 10: 15826.

1092 Tamir, T. Y., B. M. Bowman, M. J. Agajanian, D. Goldfarb, T. P. Schrank, T. Stohrer, A.
1093 E. Hale, P. F. Siesser, S. J. Weir, R. M. Murphy, K. M. LaPak, B. E. Weissman, N. J.
1094 Moorman, and M. B. Major. 2020. 'Gain-of-function genetic screen of the kinome
1095 reveals BRSK2 as an inhibitor of the NRF2 transcription factor', J Cell Sci, 133.

1096 Truong, T. H., and K. S. Carroll. 2013. 'Redox regulation of protein kinases', Crit Rev
1097 Biochem Mol Biol, 48: 332-56.

1098 Tsuchiya, Y., D. P. Byrne, S. G. Burgess, J. Bormann, J. Bakovic, Y. Huang, A.
1099 Zhyvoloup, B. Y. K. Yu, S. Peak-Chew, T. Tran, F. Bellany, A. B. Tabor, A. E. Chan, L.
1100 Guruprasad, O. Garifulin, V. Filonenko, M. Vonderach, S. Ferries, C. E. Eyers, J.
1101 Carroll, M. Skehel, R. Bayliss, P. A. Eyers, and I. Gout. 2020. 'Covalent Aurora A
1102 regulation by the metabolic integrator coenzyme A', Redox Biol, 28: 101318.

1103 UniProt, Consortium. 2023. 'UniProt: the Universal Protein Knowledgebase in 2023',
1104 Nucleic Acids Res, 51: D523-D31.

1105 Van Der Spoel, D., E. Lindahl, B. Hess, G. Groenhof, A. E. Mark, and H. J. Berendsen.
1106 2005. 'GROMACS: fast, flexible, and free', Journal of Computational Chemistry, 26:
1107 1701-18.

1108 van Montfort, R. L., M. Congreve, D. Tisi, R. Carr, and H. Jhoti. 2003. 'Oxidation state of
1109 the active-site cysteine in protein tyrosine phosphatase 1B', Nature, 423: 773-7.

1110 Venkat, A., G. Watterson, D. P. Byrne, B. O'Boyle, S. Shrestha, N. Gravel, E. E.
1111 Fairweather, L. A. Daly, C. Bunn, W. Yeung, I. Aggarwal, S. Katiyar, C. E. Eyers, P. A.
1112 Eyers, and N. Kannan. 2023. 'Mechanistic and evolutionary insights into isoform-specific
1113 'supercharging' in DCLK family kinases', bioRxiv.

1114 Wani, R., J. Qian, L. Yin, E. Bechtold, S. B. King, L. B. Poole, E. Paek, A. W. Tsang,
1115 and C. M. Furdui. 2011. 'Isoform-specific regulation of Akt by PDGF-induced reactive
1116 oxygen species', Proc Natl Acad Sci U S A, 108: 10550-5.

1117 Weisner, J., R. Gontla, L. van der Westhuizen, S. Oeck, J. Ketzer, P. Janning, A.
1118 Richters, T. Muhlenberg, Z. Fang, A. Taher, V. Jendrossek, S. C. Pelly, S. Bauer, W. A.
1119 van Otterlo, and D. Rauh. 2015. 'Covalent-Allosteric Kinase Inhibitors', Angew Chem Int
1120 Ed Engl, 54: 10313-6.

1121 Wu, J. X., Y. S. Cheng, J. Wang, L. Chen, M. Ding, and J. W. Wu. 2015. 'Structural
1122 insight into the mechanism of synergistic autoinhibition of SAD kinases', Nat Commun,
1123 6: 8953.

1124 Xiao, H., M. P. Jedrychowski, D. K. Schweppe, E. L. Huttlin, Q. Yu, D. E. Heppner, J. Li,
1125 J. Long, E. L. Mills, J. Szpyt, Z. He, G. Du, R. Garrity, A. Reddy, L. P. Vaites, J. A.
1126 Paulo, T. Zhang, N. S. Gray, S. P. Gygi, and E. T. Chouchani. 2020. 'A Quantitative
1127 Tissue-Specific Landscape of Protein Redox Regulation during Aging', Cell, 180: 968-83
1128 e24.

Yeung, W., A. Kwon, R. Taujale, C. Bunn, A. Venkat, and N. Kannan. 2021. 'Evolution of Functional Diversity in the Holozoan Tyrosine Kinome', Molecular Biology and Evolution, 38: 5625-39.

Yoshida, H., and M. Goedert. 2012. 'Phosphorylation of microtubule-associated protein tau by AMPK-related kinases', J Neurochem, 120: 165-76.

Zmijewski, J. W., S. Banerjee, H. Bae, A. Friggeri, E. R. Lazarowski, and E. Abraham. 2010. 'Exposure to hydrogen peroxide induces oxidation and activation of AMP-activated protein kinase', J Biol Chem, 285: 33154-64.

1161

1162

1163

1164

1165

1166

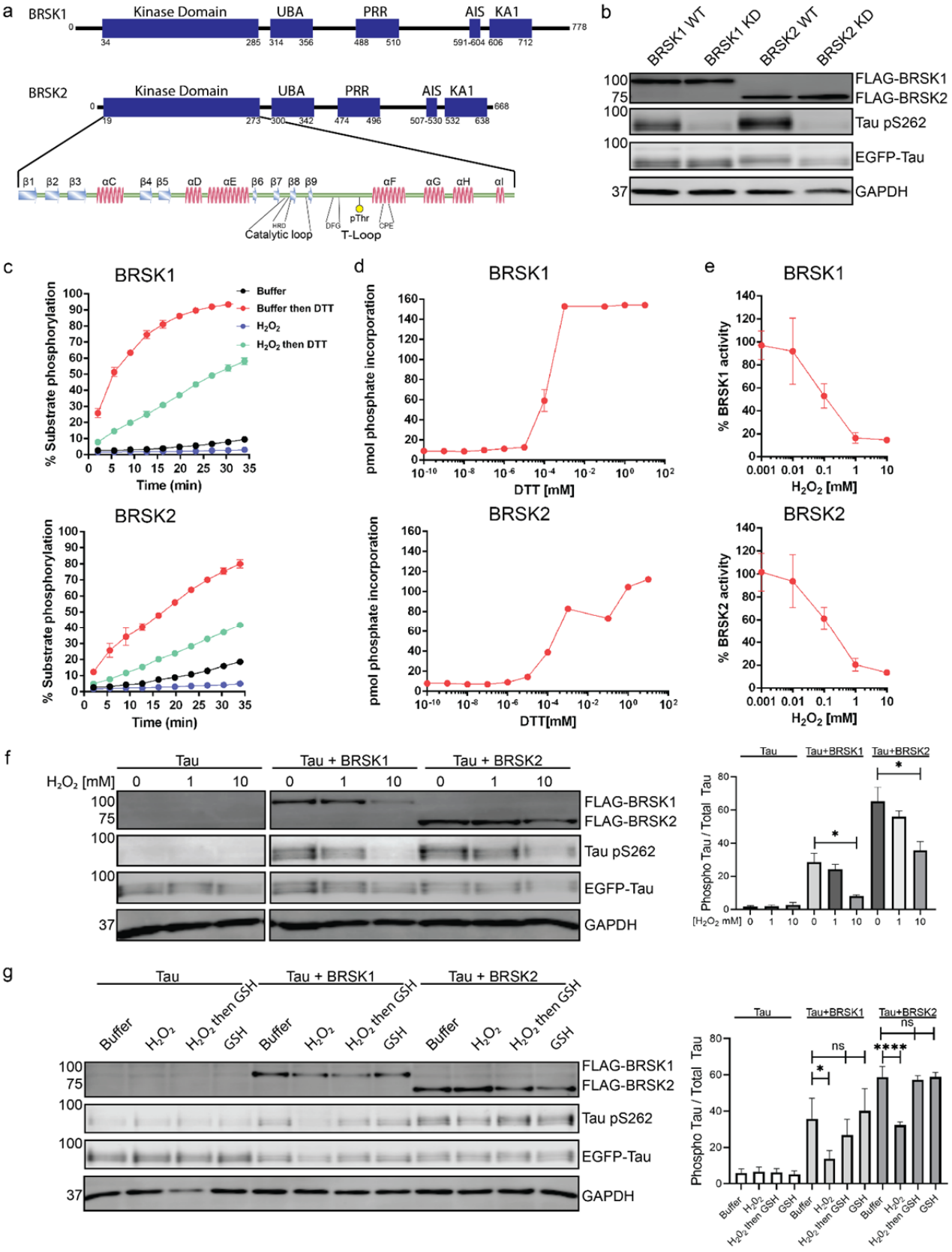

Figure 1: BRSK1/2 are redox sensitive. (a) Schematic representation of BRSK domain architecture, including Kinase domain, Ubiquitin Associated (UBA) domain, Proline-Rich Region (PRR), Kinase Associated Domain(KA1), and Autoinhibitory Sequence (AIS). (b) Real time phosphorylation of fluorescent AMARA peptide by full length BRSK1 and 2 (200 ng). BRSK proteins were incubated with buffer or 1 mM $H_2O_2$ for 10 mins, reactions were then initiated with the addition of ATP and peptide substrate in the presence (where indicated) of 10 mM DTT. Dose response curves for (c) DTT and (d) $H_2O_2$ with 200 ng full-length BRSK1 and BRSK2. All kinases assays are shown as mean and SD of three experiments. (e) Immunoblotting for BRSK dependent phosphorylation of Tau at Ser262 (pS262), from lysates of HEK-293T cells overexpressing full-length FLAG-BRSK1 or 2 (wild type [WT] or kinase dead [KD]) and GFP-Tau. (f) Immunoblotting analysis (left) of pS262 in transiently co-transfected HEK-293T cells incubated with the indicated concentration of $H_2O_2$ for 10 mins. Normalized densitometry of Tau pS262 signal (right) was calculated from 3 independent experiments. (g) Representative immunoblot (left) of transiently co-transfected HEK-293T cells treated with 10 mM $H_2O_2$ for 10 mins before the addition of 20 mM GSH. Whole cell lysates were harvested after a further 15 mins. Normalized densitometry of Tau pS262 signal (right) was calculated from 3 independent experiments.

1193

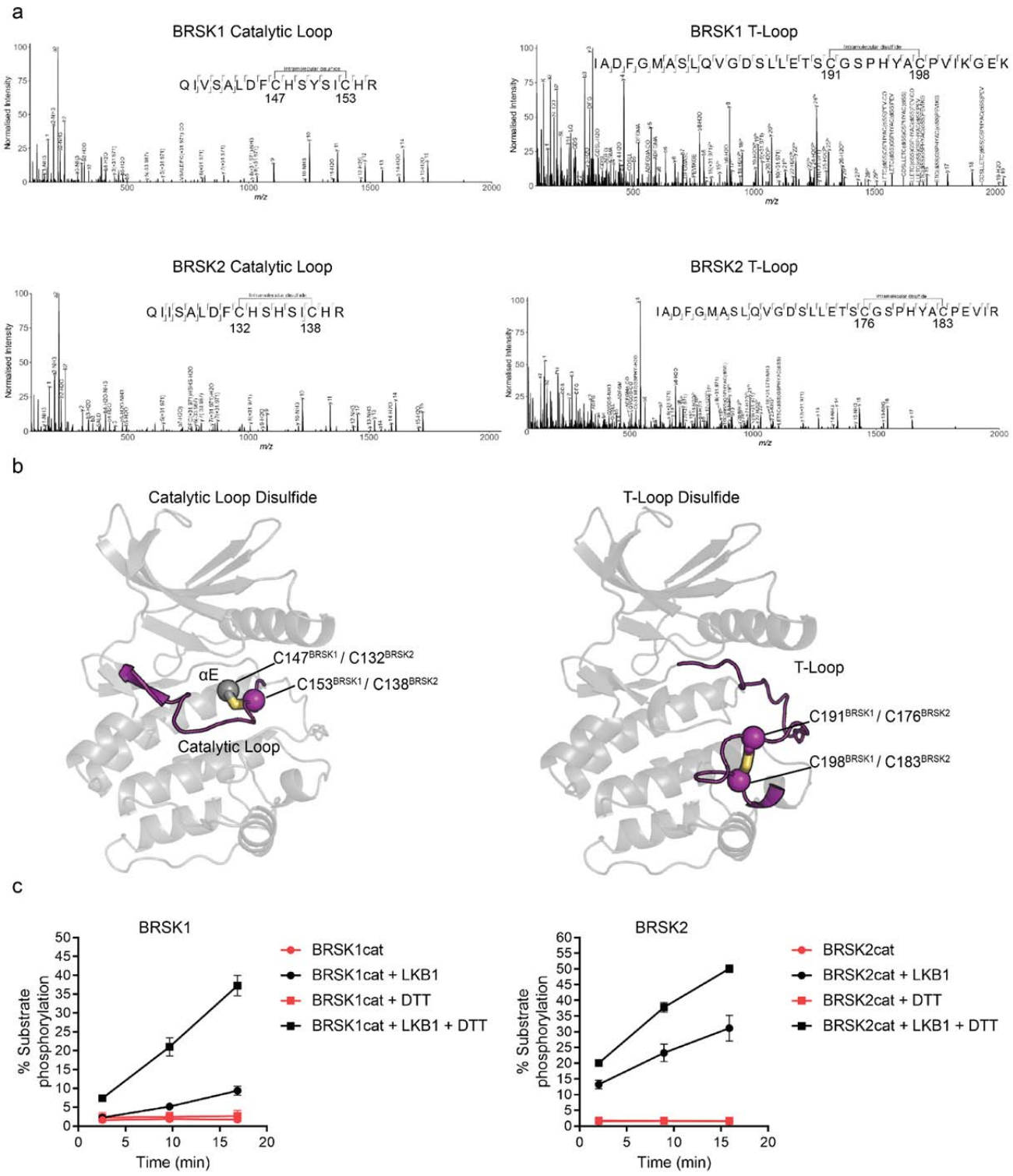

Figure 2: Intramolecular disulfide bonds form in the kinase domains of BRSK1 and 2. (a) Full length BRSK1 and 2 were affinity-purified from HEK-293T cells and subjected to LC-MS/MS analysis. LC-MS/MS spectrum mapping revealed disulfide bridges formation between $C147^{BRSK1}$ - $C153^{BRSK1}$, $C191^{BRSK1}$ - $C198^{BRSK1}$, $C132^{BRSK2}$ - $C138^{BRSK2}$, and $C176^{BRSK2}$ - $C183^{BRSK2}$. (b) Alphafold structures demonstrating the location of disulfide bonds within the kinase domains of BRSK1 and BRSK2. (c) Real time phosphorylation of fluorescent AMARA peptide by the kinase domains of BRSK1 and 2 (100 ng). BRSK1 29-358 and BRSK2 14-341 were activated by incubation with LKB1 and assayed in the presence of absence of 1 mM DTT.

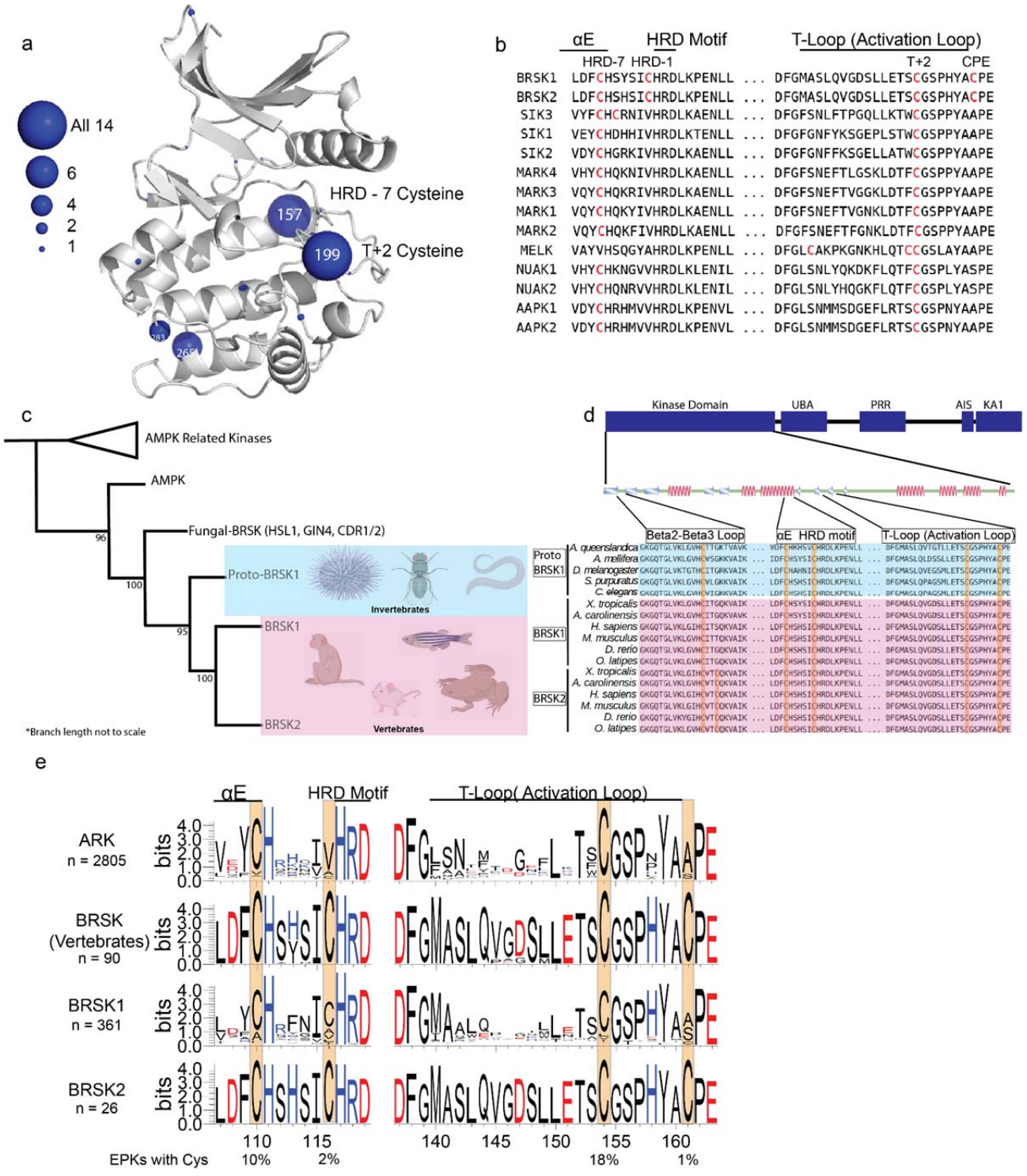


1204 Figure 3: Cysteine pairs are highly conserved within the activation segments of BRSKs.
1205 (a) Mapping of Cys residues (spheres) in the kinase domains of human ARK
1206 family members. Numbers represent the corresponding amino acid position in

PKA. Sphere size is proportional to the number of ARKs that contain a Cys at a specific site. (b) Activation segment sequence alignment of the 14 human ARKs. (c) Phylogenetic analysis showing divergence and grouping of BRSKs sub-families in different taxonomic groups. Bootstrap values are included for each clade. (d) Sequence alignment of the kinase domains of invertebrate and vertebrate BRSKs. (e) Analysis of relative amino acid conservation in ARKs and BRSKs, centered on the HRD containing catalytic loop, and the T-loop (between the DFG and APE motifs). Data is presented as HMM (hidden Markov models) Sequence Logos. The % of ePKs that possess a specific Cys is shown at the bottom.

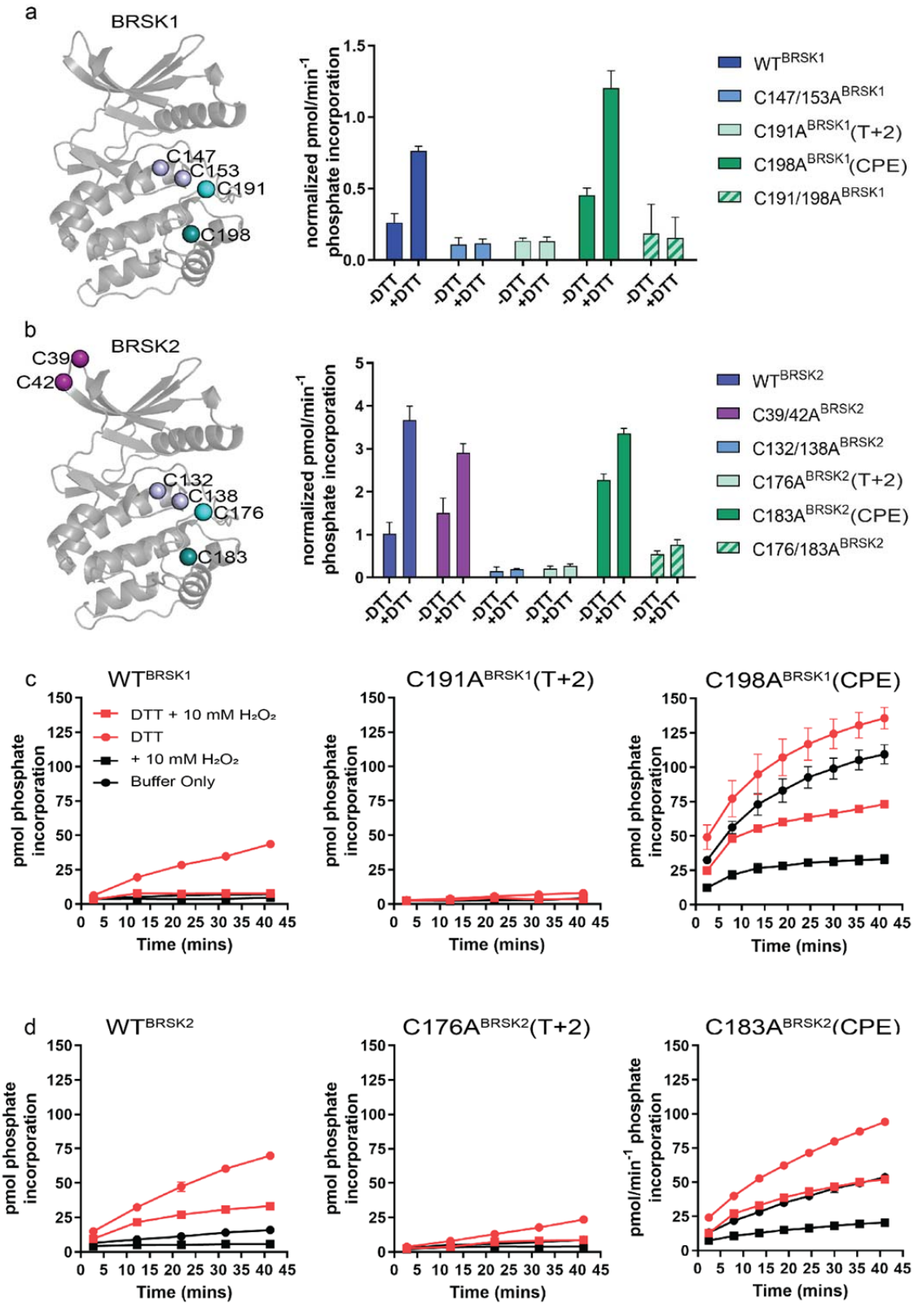


1218

Figure 4: Cysteine residues within the kinase domain fine-tune BRSK activity. In vitro kinase assays (right panels) showing normalized rates of peptide phosphorylation by WT and Cys-to-Ala variants of (a) BRSK1 and (b) BRSK2. 100 ng of LKB1 activated BRSK kinase domain was assayed in the presence or absence of 1 mM DTT. The positions of mutated Cys residues are modelled on the kinase domain as coloured spheres (left panel). Real time in vitro assays using (c) 50 ng BRSK1 and (d) 20 ng BRSK2. LKB1-activated BRSK proteins were incubated on ice in the presence or absence of 250 µM DTT for 30 mins. Assays were initiated by the addition of ATP and fluorescent peptide substrate in the presence or absence of 1 mM $H_2O_2$. All data is mean and SD of 3 experiments.

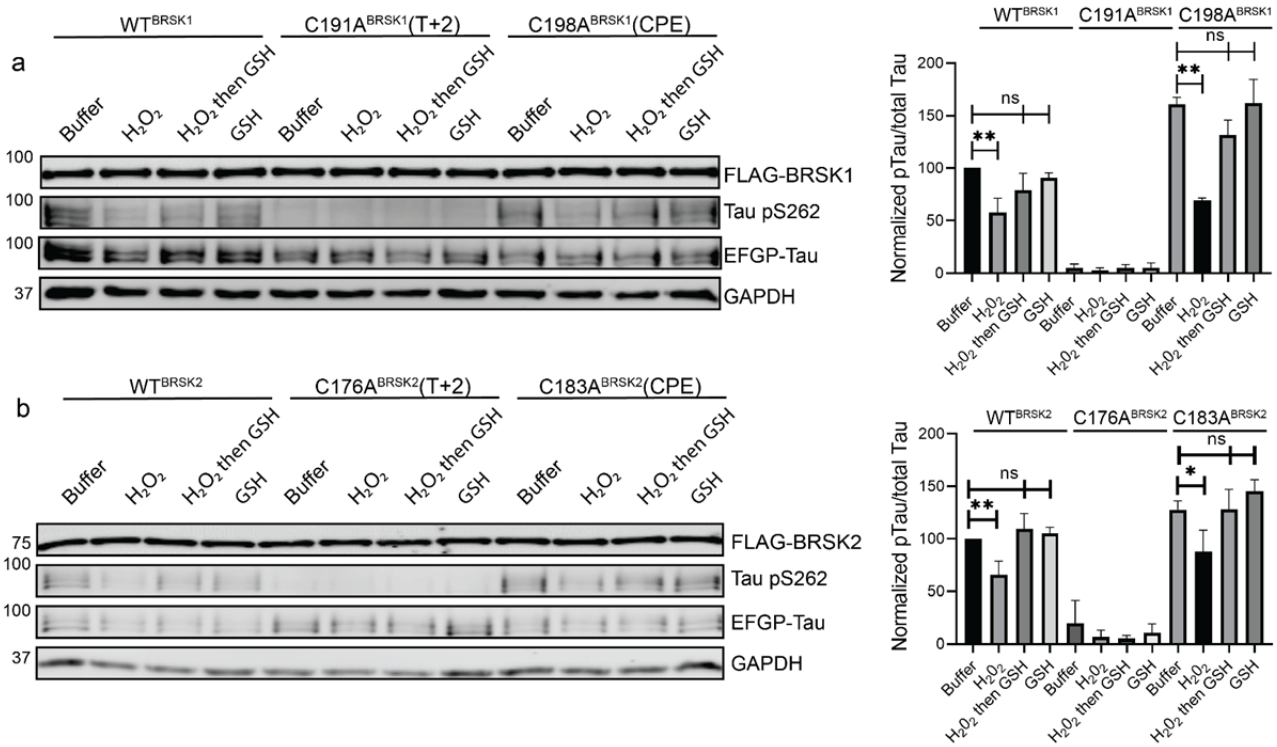


Figure 5: Impact of T-Loop and CPE Cys-to-Ala mutations on BRSK redox sensitivity in a cellular EGFP-Tau HEK-293T co-expression system. Representative immunoblot of EGFP-Tau co-expressed with WT and Cys-to-Ala mutants of (a) BRSK1 and (b) BRSK2 (left panels). Transiently transfected HEK-293T cells were treated with or without 10 mM $H_2O_2$ for 10 mins before the addition of 20 mM GSH. Whole cell lysates were harvested after a further 15 mins.

Densitometry of Tau pS262 signal (right panels) was calculated from 3 independent experiments. All values are normalized to Tau pS262 signals from control (buffer only treatment) WT BRSK and Tau co-transfections.

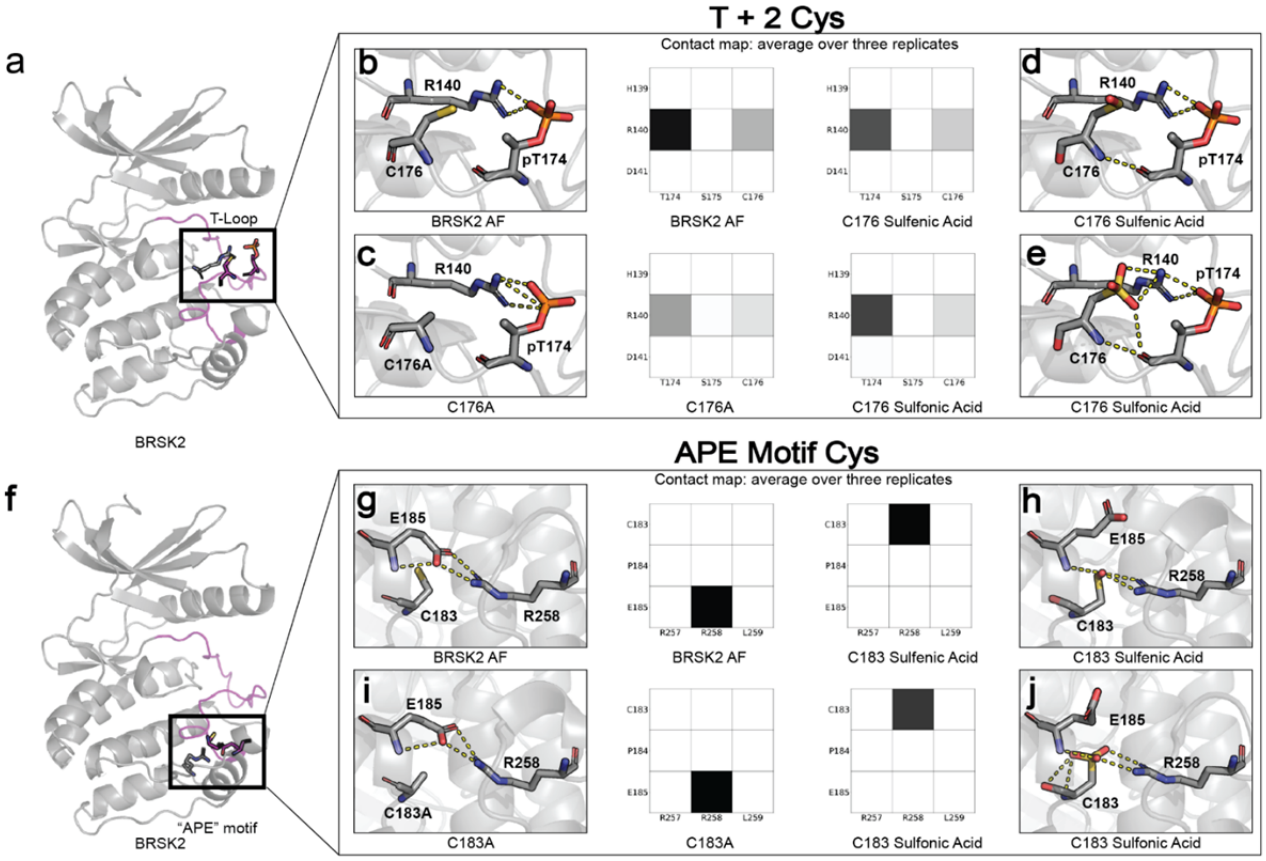


Figure 6: Oxidative cysteine modifications alter critical structural interactions required for BRSK allosteric regulation. Three replicates of 100 ns GROMACS molecular dynamics simulations were performed to evaluate the effects of cysteine mutation and oxidation. Salt bridge disruption was analyzedby generating contact maps representing the percentage of the simulation time in which residues were within appropriate distance (3 Angstroms). (a) T+2 Cys is located in proximity to the activation loop threonine in the T loop. (b-e) Evaluation of pT174-R140 salt bridge formation in wild type, C176A, and oxidized C176 BRSK2. (f) Location of CPE salt bridge within BRSK2. (g-j) Evaluation of E185-R248 salt bridge formation in wild type, C183A, and oxidized C183 BRSK2.

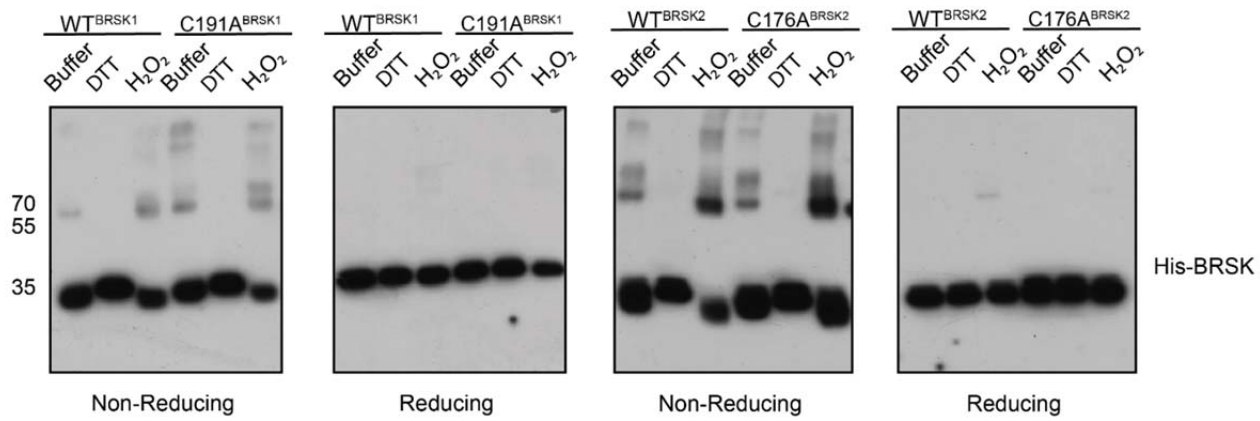


Figure 7: BRSK1/2 form limited disulfide-mediated multimers. BRSK1/2 kinase domain purified from *E. coli* were incubated with buffer, $H_2O_2$, or DTT and subjected to non-reducing or reducing PAGE to evalute the formation of intramolecular disulfide bonds.

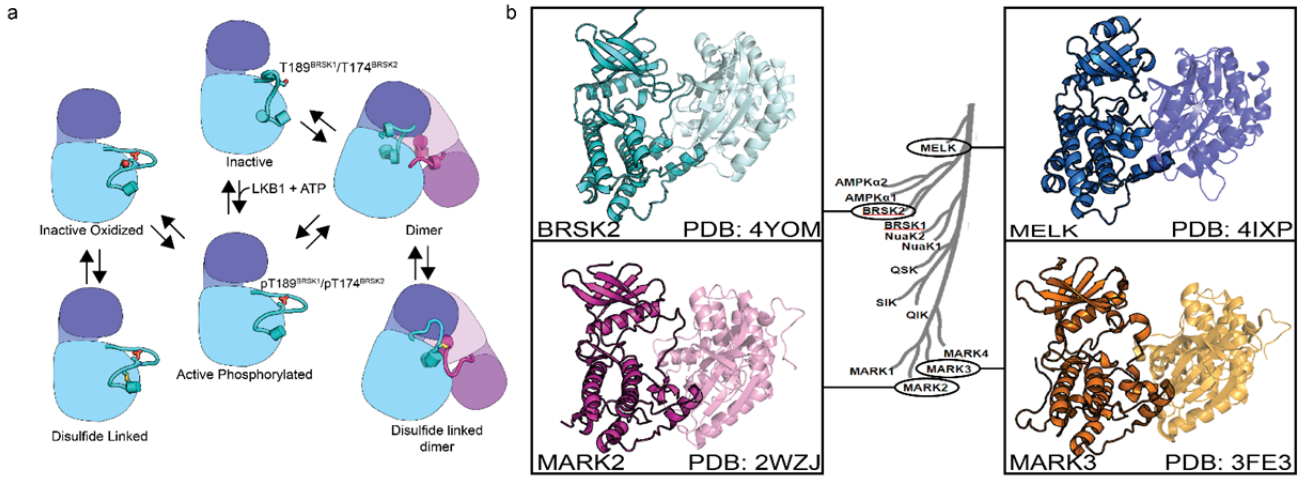


Figure 8: (a) Model of BRSK1/2 regulation. Scematic diagram demonstrating ways in which residues within BRSK kinases permit fine-tuning of catalytic activity through a variety of oxidative modifications, potentially including inter and intramolecular disulfide bonds. Cartoon representation of kinase domain with N-lobe colored dark blue/purple and the C-lobe colored light blue/purple. (b) ARK family member crystal structures demonstrate the ability to form asymetric dimers bringing T + 2 cys into proximity. Crystal structures for MARK2 and MELK both contain intermolecular disulfide bonds between T + 2 cys.

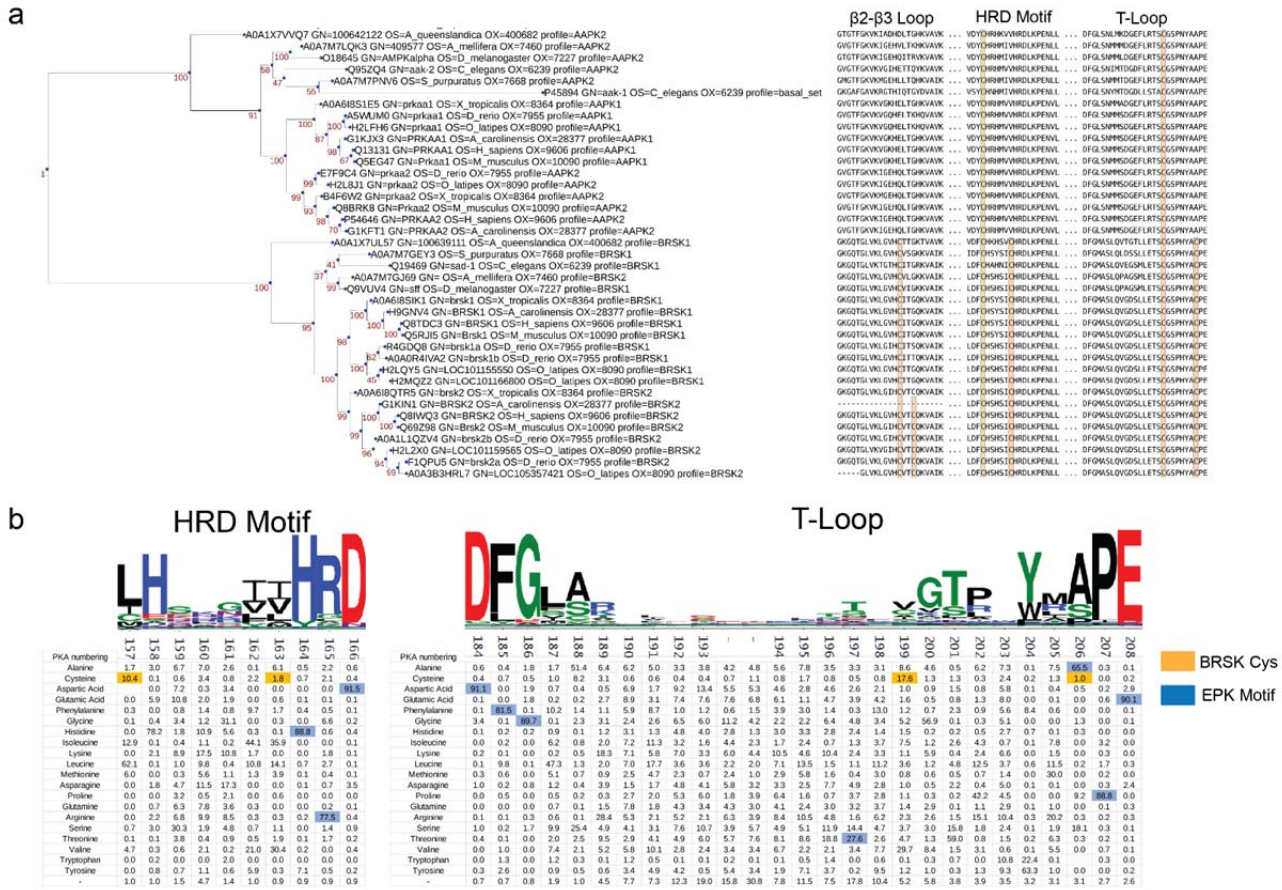


Supplementary Figure 1: Phylogenetic analysis of BRSK and the ARK family. (a) Phylogenetic analysis of the ARK family reveals that the closest relative of BRSK kinases is AMPK. The number of cysteines in the kinase domain of BRSKs increases relative to AMPK. (b) Sequence alignment and relative amino acid composition of the activation segment of ePKs (top). Data is presented as HMM (hidden Markov models) Sequence Logos. Table (bottom) depicts the frequency of an amino acid at each position along the Catalytic and T-Loop. Key Cys residues are highlighted in orange; residues highly conserved in ePK canonical kinase motifs are highlighted in blue.

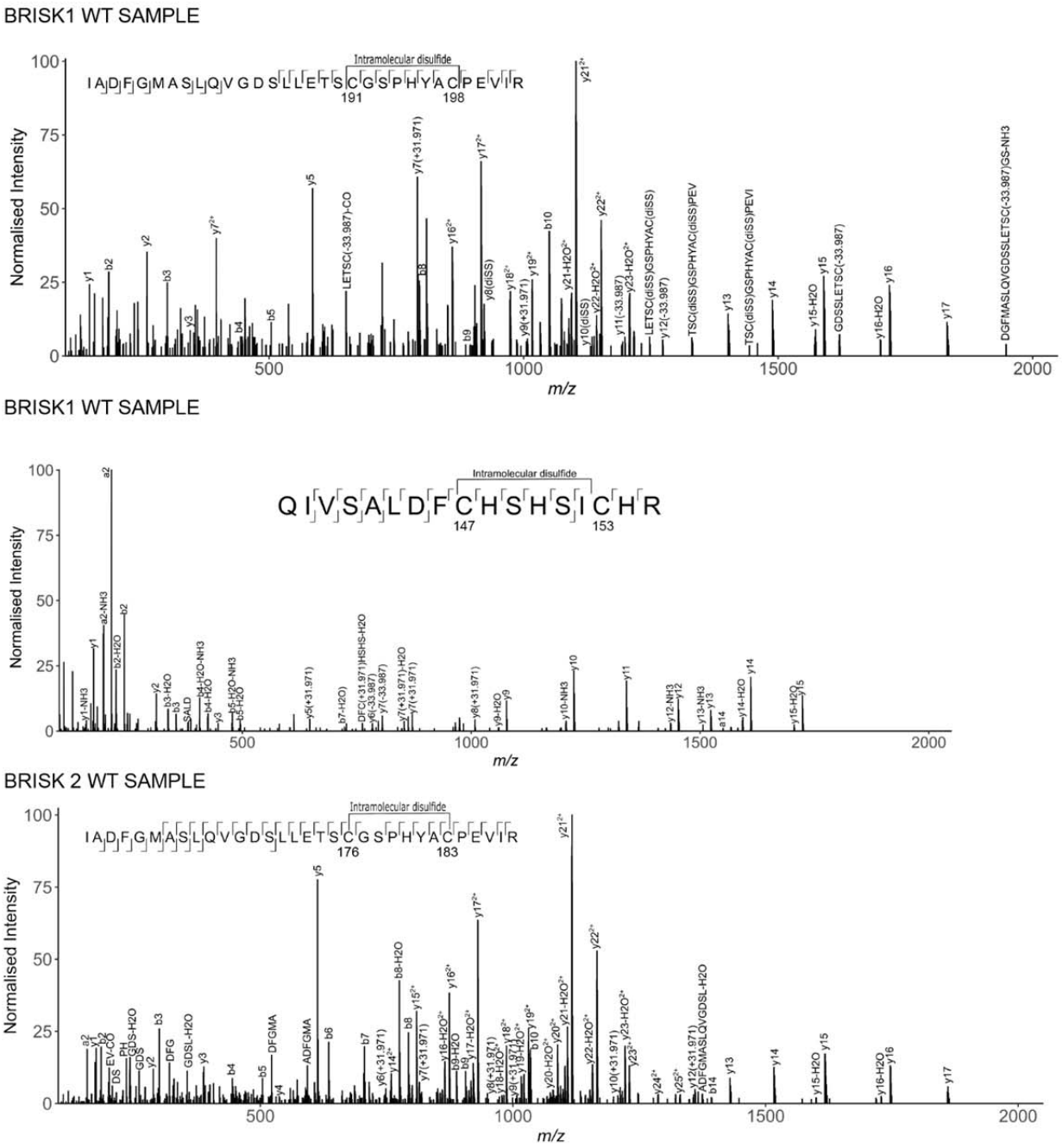


1282

1283 Supplementary Figure 2: LC-MS/MS Analysis of BRSK1/2 catalytic domians. LC-
1284 MS/MS reveals intramolecular disulfide bonds in the kinase domains of BRSK1
1285 and 2 purified from *E. coli*.

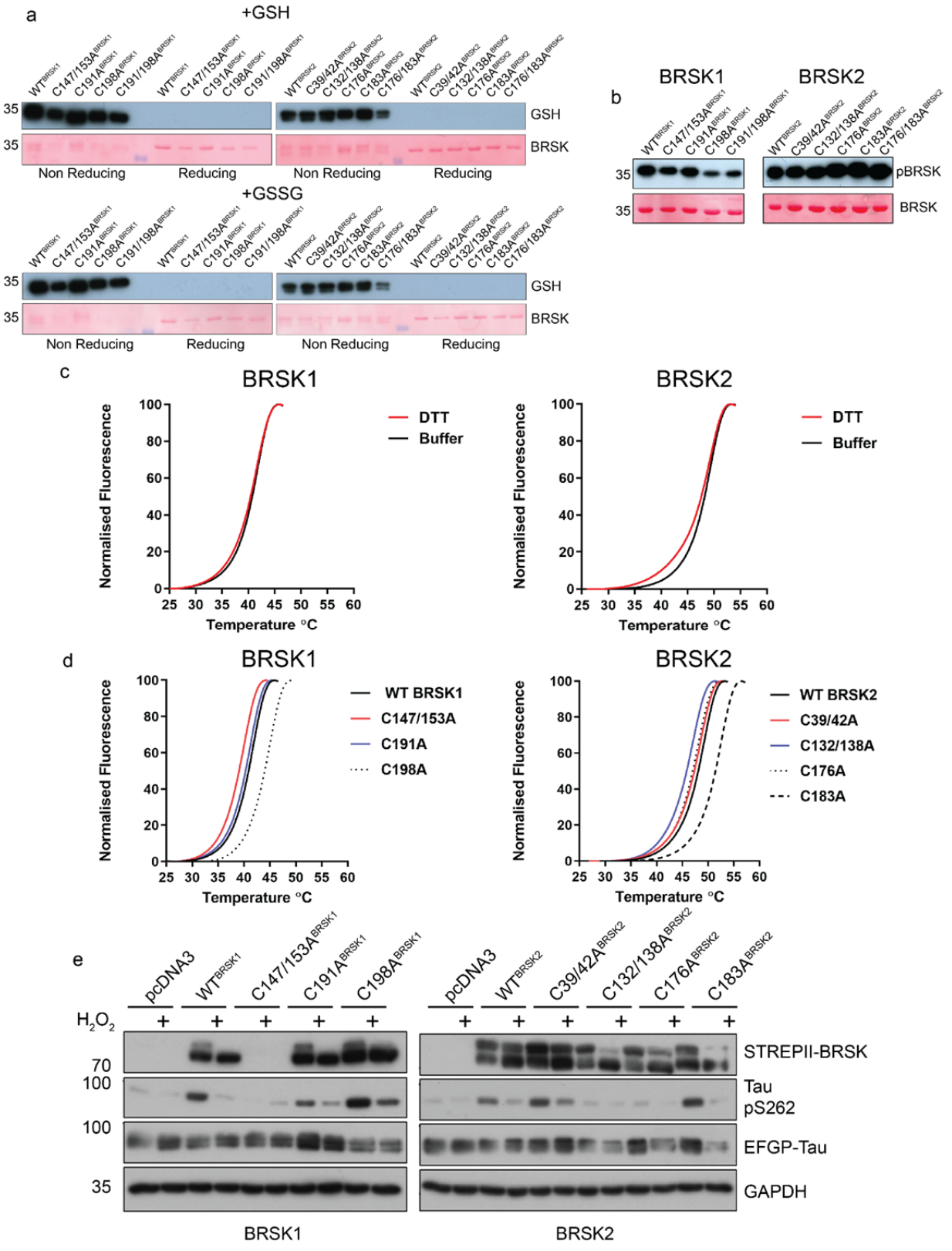


1286

Supplementary Figure 3: Biochemical analysis of BRSK Cys-to Ala mutants. (a) Immunoblot of in vitro glutathionylation of BRSK kinase domains. (b) Immunoblot showing LKB1-dependent phosphorylation of BRSK kinase domain proteins. (c) Thermal denaturation curves of BRSK catalytic domain proteins in the presence or absence of 10 mM DTT. (d) Thermal denaturation curves of BRSK catalytic domain cysteine to alanine mutants. (e) Representative immunoblot of EGFP-Tau co-expressed with full length, StWT and Cys-to-Ala mutants of BRSK1 and BRSK2. Transiently transfected HEK-293T cells were treated with or without 10 mM $H_2O_2$ for 10 mins.

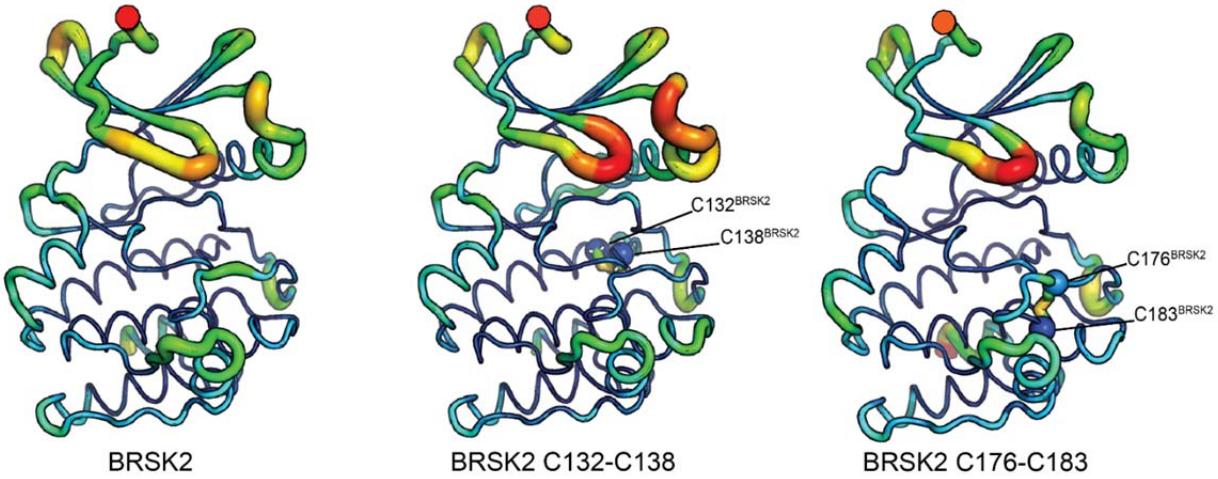


Supplementary Figure 4: Molecular Dynamics Simulations of intramolecular disulfide bonds. Simulations incorporating disulfide bonds identified in MS/MS experiments. RMSF was calculated based on three 100 ns GROMACS molecular dynamics simulations. Higher mobility is indicated by warmer colors and thickness of representation.

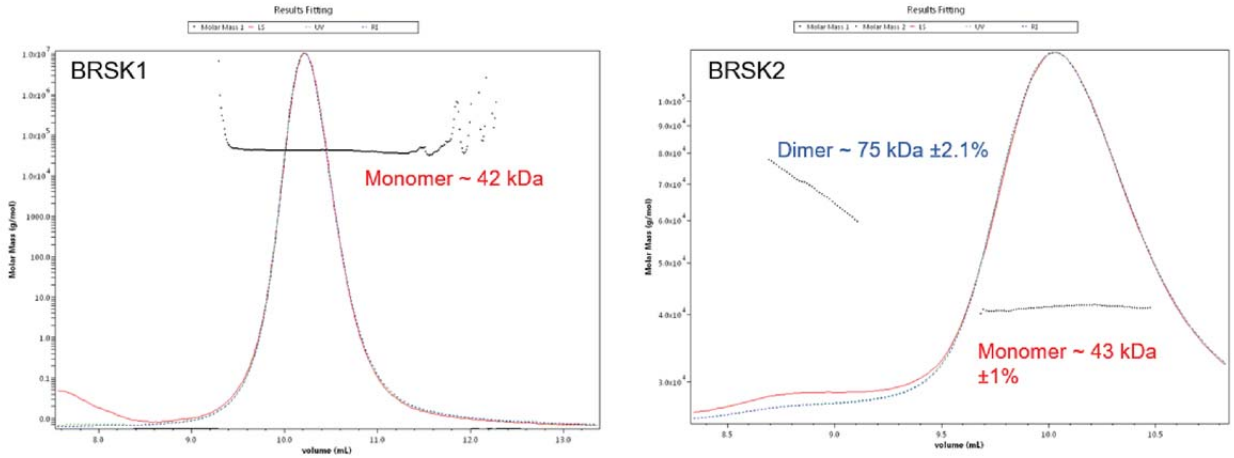


1301 Supplementary Figure 5: SEC-MALS analysis of BRSK1 and 2 kinase domains in
1302 solution.

1303

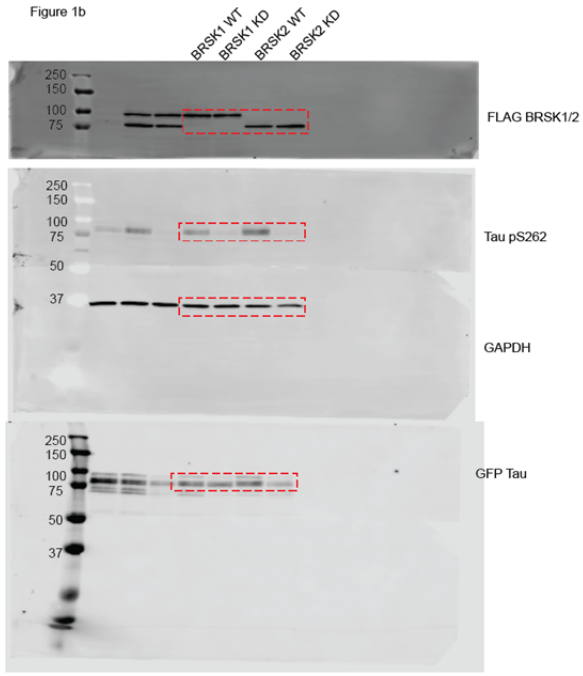


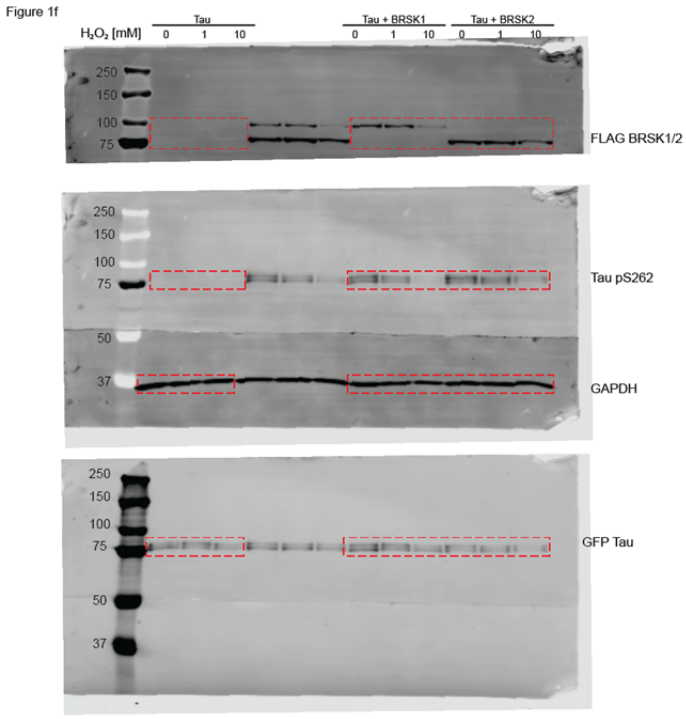


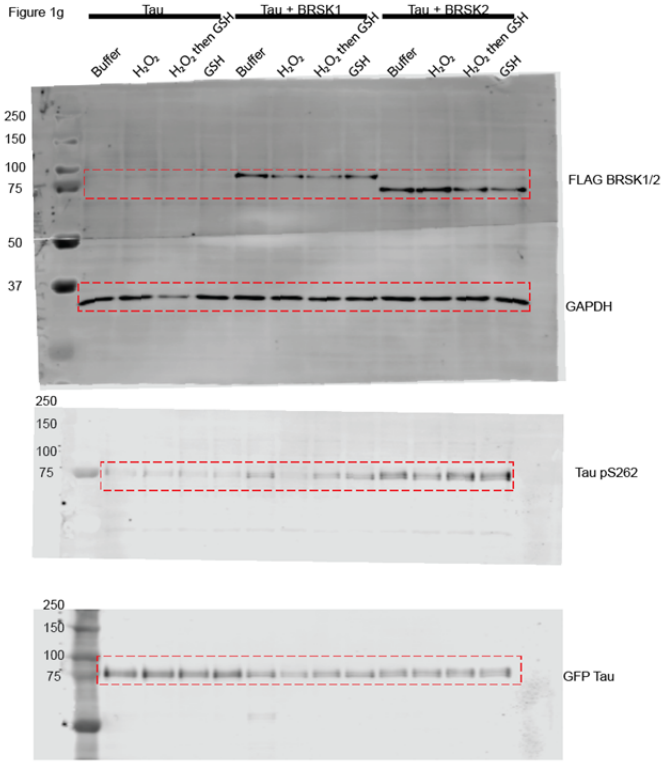


1304

1305 Source Data 1: Uncropped images from figure 1 showing changes in Tau phosphorylation in response to
1306 redox conditions.

1307

1308

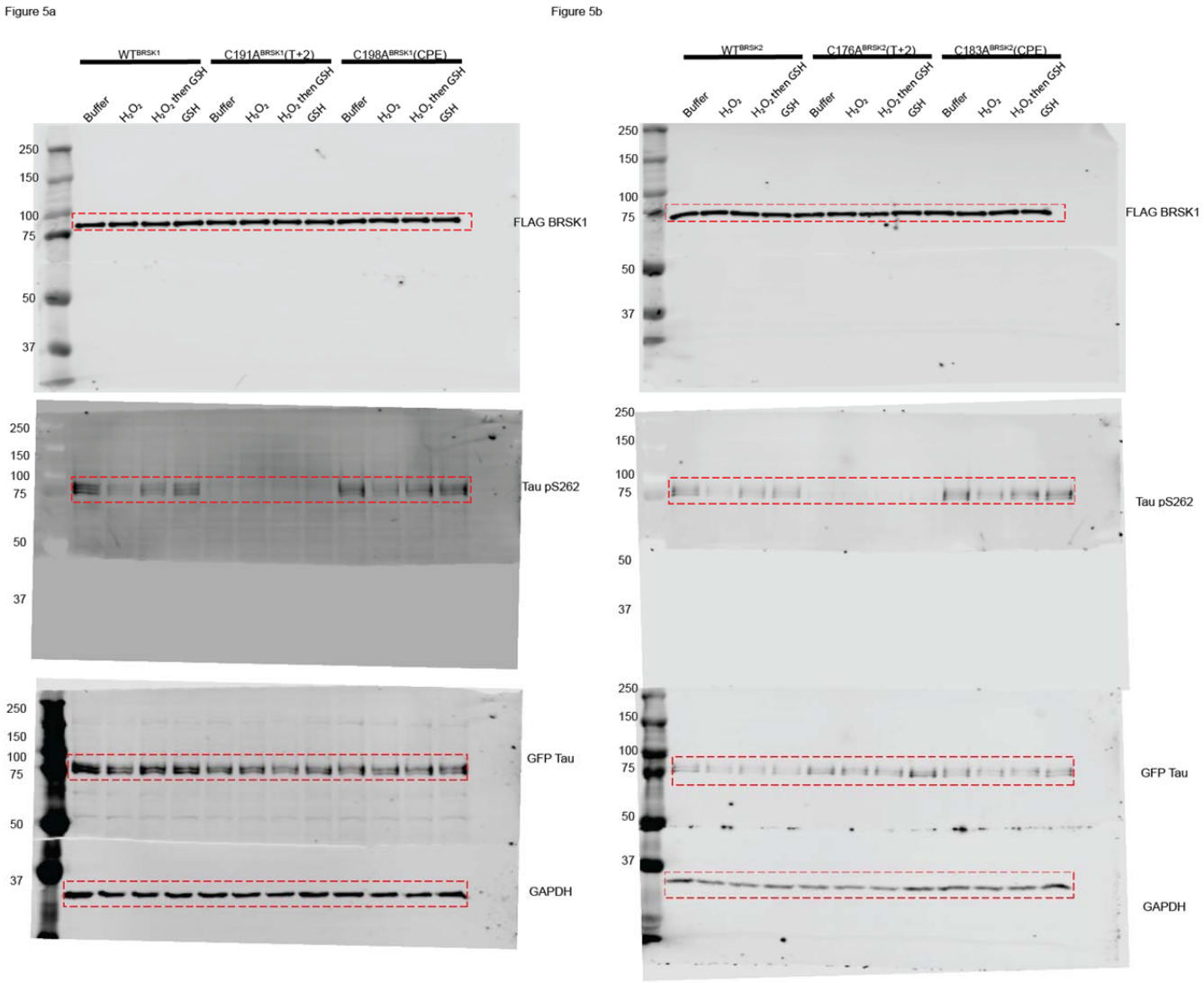


1309

1310 Source Data 2: Uncropped images from figure 5 demonstrating changes in Tau phosphorylation due to
1311 point mutations.

1312